The importance, status, and perspectives of hybrid lanthanide-doped upconversion nanothermometers for theranostics

Received 00th January 20xx,
Accepted 00th January 20xx

DOI: 10.1039/x0xx00000x

Simona Premcheska, Mirijam Lederer and Anna M. Kaczmarek*

Theranostics combines diagnostics and therapy in a single multifunctional system. Multifunctional upconversion luminescent lanthanide-doped nanothermometers for theranostic purposes offer non-invasive and sensitive multimodal performance in the biomedical field over traditional temperature measurement methods. Despite existing challenges, various studies on hybrid upconversion nanothermometers show substantial progress for (bio)imaging, temperature sensing, photodynamic and photothermal therapy, as well as drug delivery applications. The beauty of such an approach is that it unfolds possibilities to combine diagnostics and therapy in a single particle, which can modify the way certain diseases are treated, hence change the entire healthcare scene.

1. Importance of temperature measurements in biological systems

The human body is a complex medium that communicates through its temperature and its inherent thermoregulation is necessary for maintaining homeostasis. Body temperature, however, can be regarded as an overall cooperative parameter oscillating in an optimal range that depends on the fine dynamic equilibrium between the inner, core (visceral) temperature and the outer, skin (protective shell) temperature. These coupled units are in constant mutual thermal heat exchange through tissue conduction and blood convection activity, and via radiation with the environment to preserve the corporal homeothermy.[1] Many important physiological and immunological processes in living organisms are related to vital temperature fluctuations or deviations from the conventional healthy state. The deviations can be manifested as metabolic rate changes, increased or decreased blood flow, inflammation, thermal stress, etc., and these are oftentimes either generalized or localized within a restricted area depending on their origin and nature. Therefore, precise, and accurate temperature measurements are fundamental for the inspection and regulation of various biochemical processes and bodily functions. The existence of temperature gradients and significant thermal differences of cells, tissues, organs, or even extremities from their surroundings, can be a sign of potential pathological occurrences and abnormalities, therefore early screening, detection, imaging, hyper-localization, targeting, and ultimately treatment upon appropriate diagnosis is an imperative task of current scientific research. The pathology of thermoregulation can manifest as various diseases that disrupt the normal function of an organism. They can be classified as disorders with hypo- and hyperthermic occurrences. Many of these diseases have been investigated for decades and temperature measurements and imaging have been a supplementary detection and diagnosis tool in medicine.[2] Such diseases include: a general hyperthermic condition known as fever caused by either bacterial infections or inflammatory process of non-bacterial origin, then many skeletal, muscular, (cardio)vascular disorders, various types of cancer malignancy and benign tumors, diabetic neuropathies, even perforated blood vessels and blood perfusions due to lesions and fractures.[1,2] All these diseases are associated with thermal disparities observed in clinical medicine with numerous devices that have evolved with time, science, and technology.

A most striking example of minor, but detectable pathological temperature differences are those associated with the development and proliferation of cancer cells in tumor growths occurring in living organisms. Cancer cells can be defined as originally healthy cells which have mutated and have been “reprogrammed” to rapidly divide and invade their environment with the potential to metastatically spread to surrounding tissues and become lethal.[3] This is done by secretion of components to support the cell proliferation while attacking the neighboring healthy cells.[4] The tumor is usually characterized by hypoxic, ischemic, and acidic extracellular microenvironment (pH 6.0-6.8) because of the rapid cancer cell metabolism, high intracellular concentration of hydrogen (H^+) ions, hydrogen peroxide (H_2O_2), and formation of new blood vessels to supply the increased uptake of nutrients which could ultimately lead to metastasis into the blood and lymphatic circulatory systems.[3,5]

For example, it has been found that this excessive nutrient uptake and proliferation in malignant bronchial lesions causes non-trivial temperature differences in a small range of 1-2 *°C*, and malignant lesions are detected and differentiated from benign lesions with accuracy when ΔT > 1.05 °C.[6] Similar sensitive temperature differences have been found in skin temperature thermal mapping between non-melanoma lesions and melanoma metastases.[7] In another study of skin temperature in soft-tissue tumors it was obtained that even 0.2 °C is a significant difference discriminating between benign and malignant lesions in screened patients.[8] Other features of tumors include pronounced intracellular antioxidant presence, as well as a four-fold increase of the commonly present glutathione (GSH) tripeptide as compared to its usual content in normal, healthy cells.[5,9] Furthermore, temperature is also important for thermal treatment of cancer cells which manifest higher heat sensitivity and enhanced cytotoxicity to local hyperthermic exposure in the range of 40-44 °C as compared to healthy cells for a reasonable intensity and irradiation time.[10]

NanoSensing Group, Department of Chemistry, Ghent University, Krijgslaan 281-S3, 9000 Ghent, Belgium.
* Email corresponding author: anna.kaczmarek@ugent.be

Because of this, hyperthermia has been used as a supplementary treatment tool to radiotherapy and chemotherapy for drug targeting in many clinical trials and has been reported to have an influence on tumor immunogenicity, pro-inflammatory cytokine activity, tumor blood perfusion, and gene expression, all of which accompany and impact the cancer pathogenesis.[11,12]

More examples of studies highlighting the importance of monitoring delicate temperature changes *in vivo* include detection of intracerebral temperature during episodes of induced focal seizures in rats being 0.3 °C higher than the core temperature, an occurrence attributed to increased blood flow to the affected brain site of the induced seizures,[13] then measuring sensitive temperature differences in joint inflammation and rheumatoid arthritis cases in humans,[14] detection of temperature variations in conditions with ambiguous clinical symptoms such as vasculitis,[15] registering temperature in peripheral vascular disorders in ranges as small as 0.7-1 °C when compared to surrounding healthy tissues,[16] hyperlocal temperature gradients in various types of cancer, and many more. Even though a lot of existing challenges and technical aspects are yet to be resolved for clinical monitoring applications, temperature in biological systems is crucial for maintaining the life-preserving functions and offers a modality that can be coupled and further exploited into state-of-the-art multimodal systems for sensitive *in vivo* real-time monitoring of emerging temperature changes.

Allowing researchers and medical professionals to pinpoint these temperature changes down to their development at the nanoscale ground-zero, through judiciously engineered nanomaterials exhibiting temperature-dependent spectral responses in the physiological range (20-50 °C), remains a multidisciplinary challenge. The thermal detection and tracing of remotely localized physiological changes has the future potential to be used as a rudimentary approach for diagnosis of many diseases accompanied by substantial but subtle temperature changes in the affected tissues and organs, especially in cases where traditional bioimaging has limited sensitivity and applicability.

Such high-performance materials class, demonstrating a promising behavior in tackling these challenges, are the hybrid lanthanide-doped luminescent upconversion nanomaterials bearing a temperature sensing modality within their structure. These hybrid nanothermometers are advantageous over classical purely inorganic particles due to their modifiable and multifunctional structure i.e. incorporation of biocompatible shells, voids, and frameworks with the ability to accommodate, carry and deliver cargo through safe, non-toxic, and robust platforms depending on the projected application.

2. Temperature measurement methods currently used in clinical medicine for imaging and diagnosis

Numerous temperature measurement devices and methods are currently being used in medicine for imaging and diagnosis of patients and they all have their own advantages and significant limitations when it comes to biological and clinical requirements.[1] From technical and practical aspects to complex and costly handling and maintaining, to continuous advances in technology and materials science, to increasingly demanding medical needs, even to rigorous performance features, these thermometry methods are proving to have many downfalls and oftentimes fail to meet the delicate requirements of human evolution. The thermometry/thermography devices applied in medical practice can be classified in a variety of ways, i.e., depending on the physical approach (contact and contactless), on the output signal form (electric and non-electric), on the measured physical variable exploited to detect temperature, on the operating range, etc.[17] Various temperature-detection and monitoring methods applied in clinical practice are briefly described in Table 1.

One important aspect influencing the thermometer choice is the measurement uncertainty to which the temperature should be determined, as well as the nature of the condition being followed. This is usually a compromise, however, in modern medicine it is desirable to have a thermometer performing with uncertainty of the lowest possible range to register the slightest temperature variations. Measurement uncertainty derives from the notion that the measured value of a physical quantity is inherently accompanied by measurement errors due to imperfections of various types.[17,18] Measurement errors cause deviations of the measured value from the true value of the physical quantity and since all errors cannot be entirely predicted and eliminated, the objective is to assess and minimize them as efficiently as possible.[17] In a manner, the overall temperature measurement uncertainty can be regarded as a cumulative parameter which includes a few parameters and figures of merit, characterizing the thermometer calibration and performance, implicitly its application too. The measurement values and uncertainties are reported in temperature values according to a specific measurement model defining the accuracy, precision, sensitivity, selectivity, and resolution of the thermometer.[17] The measurement uncertainties of a few thermometers commonly exploited in clinical practice are overviewed and compared in Fig.1.

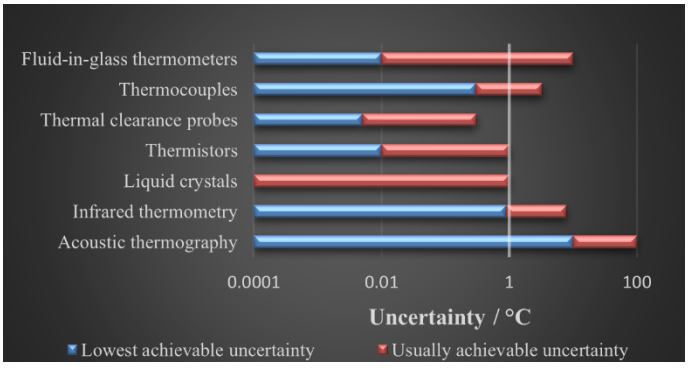

Figure 1 Chart roughly depicting the temperature measurement uncertainties of a few temperature measurement methods on a logarithmic scale. Adapted from Reference [18], with permission from Elsevier.

Table 1 Temperature measurement methods used in clinical practice and their brief descriptions

Temperature measurement method	Description
Fluid-expansion / fluid-in-glass thermometers	Probably the oldest and most exploited temperature measurement tools. Despite their wide use, their handling requires caution and their contact-based approach with skin and body cavities is rather invasive and unpleasant. They suffer from low spatial and thermal sensitivity.[1]
Thermocouples	These devices exploit the thermoelectric (Seebeck) effect of two metal conductors in a carefully constructed circuit. The conductive elements must satisfy certain conditions to be coupled for biomedical purposes.[1,17] Their disadvantages include nonlinear dependence of circuit voltage on temperature, distance-dependent performance, as well as low sensitivity.
Thermal clearance probes	Consist of arranged series of thermocouples, connected to a heater applied to the skin for measuring thermal conductivity of blood flow, however, their distance-dependent performance is influenced by their design, the type of skin being investigated, and the depth, size, and number of the blood vessels in the concerned area.[1]
Thermistors	These devices measure the electrical resistance of a semiconductive material as a function of the temperature only after establishing a calibration curve relationship which is unique for each device. Disadvantages include invasiveness, fragility, need for insulation, and narrow operating ranges.[1]
Liquid crystals in liquid crystal thermography	These cholesteric materials are applied over the concerned body area, usually arranged/attached on a sheet, and change their color depending on the heat emanating from the skin. Their disadvantages include low spatial resolution, low thermal sensitivity, and non-linear dependence of optical response to temperature.[1]
Radiation thermometry	This contactless technique exploits the fact that all objects emit EM-radiation from their surface, however, its performance depends largely on the surface emissivity and the environment, as well as the technical operating conditions.
• **Infrared radiometers**	Measure temperature with sensitivity in the range of 2-25 μm. They are portable; however, their sensitivity varies with device design and their handling requires experienced personnel. These radiometers are usually not used separately but in combination with a thermal imaging method.[1]
• **Infrared (IR) thermography**	Probably the most widely exploited contactless technique in clinical imaging and diagnosis. The setup consists of a scanning unit of optical elements that captures the thermal radiation emitted by the subject and an infrared detector that converts the optical signal to electrical. The output, so-called thermogram, is recorded and displayed on a screen by advanced image acquisition and image processing electronic unit. This complex instrumentation requires experienced handling, usage of image databases, and cautious image analysis. Disadvantages include relatively high costs for maintenance, variable thermal sensitivity depending on the type of detector used, and strictly controlled operating and imaging protocols. Moreover, the subjects must follow a strict procedure in terms of clothing choice, and make-up application prior to imaging.[2]
• **Microwave thermography**	Utilizes the thermally dependent emissivity of the skin in the microwave region of the EM-spectrum on the basis that human tissue is optically transparent to microwaves. Even so, this method suffers from low tissue radiation intensity and environment-dependent wave propagation.[1]
• **Acoustic thermometry (Ultrasound-based)**	This contactless technique is divided into active and passive methods measuring the echoed radiofrequency signal from the heated tissue upon transmission of signal, and measuring the signal being spontaneously emitted from the heated tissue, respectively. Drawbacks include temperature-dependent speed of sound, medium-dependent wave propagation, wave backscattering, and high measurement uncertainty.[19]
Magnetic resonance (MR) thermometry	This famous non-invasive technique is initially an imaging technique that includes a few methods for simultaneous temperature monitoring with the most exploited being proton resonance frequency (PRF) shift, T_1, T_2, temperature-sensitive contrast agent methods, etc. Even though the various methods generally offer good soft-tissue contrast and high sensitivity, their usage is complex, costly, tissue and subject-dependent, and differs on whether there is a requirement for a relative or an absolute temperature change measurement.[20]

***X-ray mammography**	Although not a temperature measurement technique on its own, this imaging method is primarily and most notoriously used for diagnosis of breast cancer. It utilizes ionizing radiation and very invasive breast tissue handling. It is not recommended for pregnant patients and suffers from a high rate of false positive and false negative results. It requires costly instrumentation, specialized personnel, it is unpleasant, and is characterized by low sensitivity in patients with dense breast tissue.[21] Recently, IR thermography has been applied as an alternative method for imaging and diagnosis of breast cancer due to the hyperlocal temperature variations of cancer cells, however the thermal sensitivity is low when the malignancies are located deeper in the tissue.[2]

3. Luminescence nanothermometry as an emerging alternative

Thermometry as a method of registering and monitoring temperature has been employed from ancient times and has advanced significantly since the first attempts and primitively constructed devices. Nowadays, temperature sensing probes have made, and continue to make, substantial technical and applicational progress, and have significantly challenged and outperformed their predecessors. Such cutting-edge precedent has been set by luminescent temperature sensors already meaningfully developed and investigated over the course of the last two decades.[22] Luminescence nanothermometry, broadly classified under optical nanothermometry techniques, involves measuring spectral response of an optically irradiated sample induced by temperature variations. The temperature sensing properties of such probes result in thermal images derived from the fine, directly proportional influence of temperature variations on the luminescence properties.[23]

Luminescence nanothermometry as a fast-emerging and highly promising alternative to the classical thermometry aims to eliminate the disadvantages of classical thermometry such as its contact-based invasive approach to the affected area, low spatial resolution and thermal sensitivity, limited applicability, and go a step further towards stability, robustness, specificity, and standardized reproducibility for theranostic purposes.[5,24] Of current featured focus are the core-shell hybrid silica-based, lanthanide-doped upconversion luminescent nanomaterials which attribute their optical behavior to the exceptionally shielded nature of the $4f^n$-orbitals of the lanthanide ions with an abundance of ladder-like close-lying energy levels in their electronic structures and sharp electronic transitions between energy levels. The hybrid structures offer the benefit of unconventional fusion of inorganic and organic components, each carrying moieties with advantages that could be exploited for a specific purpose yielding overall improved performance of the luminescent nanothermometers. The theoretic background, basics, and various types of luminescence thermometry are discussed in detail in the next section.

4. Photoluminescence

Luminescence is the spontaneous emission of light by a substance, it is also referred to as cold-body radiation. There are various types of luminescence, however, in this article we will focus on photoluminescence. Photoluminescence describes the process of light absorption and emission by any type of matter. There are different mechanisms that can be involved in the photoluminescence process, hereby a spotlight is put on upconversion (UC) exploited for luminescence thermometry, which is the scope of this feature article.

Types of photoluminescence thermometry/mechanisms

To this day the mechanisms and principles of photoluminescence are not completely understood and a correct prediction of all phenomenological and optical properties of materials is challenging. This makes the design and tuning of temperature sensors a sophisticated task. The basic mechanisms will be described in the following paragraphs, with a distinct focus on UC systems.

Downshifting

Downshifting involves one high-energy photon, usually UV, that is absorbed by the material. The energy of the photon is then converted and a photon with lower energy and higher wavelength is emitted. This process is usually in need of a high absorption coefficient, narrow emission band, and good separation between emission and absorption band.[17] Typical downshifting materials are quantum dots, organic dyes, and lanthanide ions with a focus on transition metal ion activators. For years research has been heavily focused on downshifting systems, resulting in good understanding of downshifting materials and internal quantum efficiencies of higher than 90 %.[17]

Upconversion

Upconversion (UC) is the process in which two or more photons are sequentially absorbed and converted into one shorter wavelength photon.[17] This means that low-energy photons, usually IR, are converted into higher-energy photons, usually visible light, through UC. This conversion can be described by five mechanisms: excited-state absorption (ESA), energy transfer upconversion (ETUC), cooperative sensitization upconversion (CSUC), cross-relaxation (CR), and photon avalanche (PA).[17,25,26] The mechanisms are schematically shown in Fig.2. Lanthanide-doped UC materials are extensively used because they offer a great number of long-lived electronic states at various energies.[17] Upconversion suffers from a small

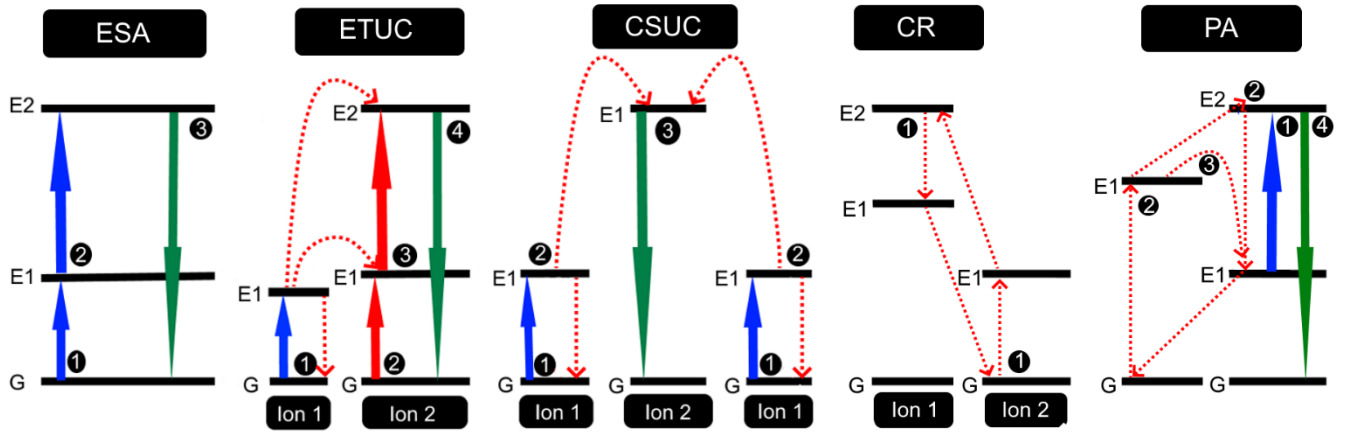

Figure 2 Mechanisms of upconversion: excited-state absorption (ESA), energy transfer upconversion (ETUC), cooperative sensitization upconversion (CSUC), cross-relaxation (CR), photon avalanche (PA). Blue arrows represent photon excitation, green arrows stand for photon emission and red arrows depict energy transfer (followed by excitation).

internal quantum efficiency with the largest efficiencies around 6.8 % for lanthanide-doped fluorides.[27]

Excited-state absorption is the successive absorption of photons by one lanthanide ion.[25,26] This successive absorption is possible due to the ladder-like energy level structure as it is present in only a few lanthanides, namely Er^{3+}, Ho^{3+}, Tm^{3+}, and Nd^{3+}. The sequential photon absorption is possible because of the equal energy from the ground state (G) to the first excited state (E1), and from the first to the second excited state (E2). The first absorbed photon excites the ion from the ground to the first excited state, which is an intermediate state. Due to the inherently long lifetime of the intermediate energy state of lanthanide ions, the probability of the promotion to the second excited state is raised significantly. Therefore, a sequential absorption leads the ion to an excitation into the second excited energy state. Upconverted emission is emitted from the second energy state. The efficiency of this upconversion mechanism is independent of the dopant concentration due to the single ion nature.[25,26]

Energy transfer upconversion (ETUC) involves two ions that are in close proximity to one another, they are referred to as the sensitizer and the activator.[17,25,26] The sensitizer (ion 1) absorbs a photon and is excited from the ground state G to a metastable first excited state E1. The energy is then transferred successively to the activator (ion 2) which is excited from the ground state to its first excited state and then further to its higher lying second excited state E2. Each time the sensitizer relaxes to the ground state after the energy transfer (ET). The distance between the neighboring atoms is strongly influenced by the doping concentration; a high sensitizer-activator concentration leads to a short average distance and vice versa.[25,26,28] The efficiency of this process is determined mainly by the average distance between the dopants and diminishes quickly with a distance shortening, leading to concentration quenching.[25,28] This will be described later. The most efficient UC systems, namely Tm^{3+}-Yb^{3+}, Ho^{3+}-Yb^{3+}, and Er^{3+}-Yb^{3+}, are utilizing the two-ion system with Yb^{3+} as a sensitizer since it enhances the absorption at 980 nm excitation as Yb^{3+} has a high absorption cross-section in the NIR region and cross-relaxation is not significantly pronounced.[17,25] Single-lanthanide systems can also work with this mechanism as the ions can work both as sensitizer and activator.[25]

Cooperative sensitization upconversion (CSUC) involves three lanthanide ions with two of them being identical.[25,26] The identical ions (designated as Ion 1 in the figure) represent the sensitizers which are excited from their ground state G to the excited state E1 by a photon. Both ions transfer their energy to the activator (Ion 2), simultaneously and cooperatively. The sensitizers then relax to their ground states again and the activator is lifted from its ground state G to its excited state E1. After emitting an upconverted photon the absorber relaxes back to its ground state. Since it involves quasi-virtual pair levels, the CSUC process is usually of significantly lower efficiency than the ESA or ETUC processes.

Cross-relaxation (CR) is a deleterious process that does not lead to emission.[25,26] It involves two ions that can be of the same or different kind. The first ion is in its second excited state and transfers its energy to the second ion. The second ion is lifted to its first excited state E1, whereas the first ion relaxes to its first excited state E1. Since CR is the result of ion-ion interaction, the main influence is that of the dopant concentration, leading to concentration quenching, described later. Energy back transfer is similar to the absorbed energy of the photon being transferred back to the sensitizer, leading to energy migration and/or quenching.

Photon avalanche (PA) produces upconversion only above an excitation power threshold after which the intensity of the photoluminescence increases orders of magnitude.[25,26] PA is a looping process of two ions that involves both ESA and CR. First, the ESA process elevates the second ion from its non-resonant first energy level to the emitting second energy level. After a cross-relaxation with Ion 1, both ions are at their first energy levels. The last step of the loop is that Ion 1 transfers its energy to another Ion 2, populating its first energy level. The looping effect results in two ions of type 2 in their first energy state, versus one ion of type 2 at the beginning of one loop. It will create 2^n ions (with n being the number of loops) of type 2 at

their first energy state, causing an avalanche and PA UC emitting from the second energy level.

Types of read-outs in nanothermometry

Different types of read-out methods rely on a variety of mechanisms and properties of the material and/or systems involved. The types of nanothermometry read-outs are shown in Figure 4. Additionally for biomedical applications, the developed nanothermometers must be non-toxic and biocompatible.[25,27] For reliable temperature determination and read-out, the photoluminescence mechanisms present in the respective materials must be understood to utilize the correct formulas and models for the calculations. Important performance parameters will only be discussed for ratiometric nanothermometry in the interest of this work.

Temperature determination based on the absolute temperature is a fast and easy approach. The change of the intensity of a single band with varying temperature is based on non-radiative energy transfer and is utilized by most quantum dots (QDs) or organic dyes. However, the emission is highly dependent on the physical and (bio)chemical environment, making this type of read-out unreliable especially *in vivo* and *in vitro*.[24] Temperature read-outs that are based on a single transition band can also be affected by alignment, opto-electronic drift of the excitation source and detectors, or quenching processes.[24,29]

For luminescence lifetime measurements, the decrease in intensity with time is measured.[17,24] A measurement can be divided into three periods: the excitation pulse, the rise time, and the decay period.[17] For lifetime measurements only the decay period (called "dead time") is used since for the first two periods sophisticated instruments must be used. It measures the non-radiative rates and energy transfers. Luminescence lifetime overcomes limitations of the physical and (bio)chemical environment as the lifetime is an intrinsic property.[24] Lifetime measurements are also considered to be self-referencing and require only the monitoring of one emission band.[17] A pitfall of lifetime measurements is that they rely on expensive and sophisticated fast detectors or time-gated detection and the temporal resolution is comparably low.[24] Another common issue is that the processing of the data is another source of error and can be challenging. Thermometry based on this type of read-out has been utilized for organic dyes and lanthanide-doped nanoparticles but is still rarely studied. Perhaps in the future, it will become more widely investigated.

Both types of read-outs utilize electron-phonon coupling to determine the temperature.[24]

Bandwidth-based measurements with semiconductor nanocrystals use the homogeneous broadening of the peaks with temperature. Spectral shift utilizes the shift of the band position with temperature to determine the latter. This type of measurement investigates either semiconductor nanocrystals or quantum dots (QDs). Both approaches overcome the limitations of single intensity-based thermometry but have major pitfalls. Spectral overlap and autofluorescence are troublesome features of this kind of read-out technique. Additionally, both techniques require high resolution and therefore expensive equipment.

Ratiometric nanothermometers are considered to be the most promising candidates for temperature determination as they balance measurement cost, reliability, and speed of detection.[30,31,32] This method is commonly used for Ln^{3+}-doped nanoparticles, and it is based on the variation in Boltzmann distribution with temperature and thermally induced energy transfer between energy levels. The thermal readout of *delta* (Δ) is not significantly influenced by the physical and/or (bio)chemical surroundings because they influence both peaks equally. When their ratio is calculated this influence is canceled out and ratiometric measurement is therefore considered to be the most robust of all techniques.[25,29] It should be pointed out that the read-out, e.g., the shape of the peaks, seems to be affected by the tissue, local concentration of the nanothermometers, and the excitation intensity.[24] As this leads to artifacts and errors in the determination of the temperature, future research will have to focus on the elimination of these issues, establishing standards for measurement and data processing and presentation.

The ratio in intensity between the thermally coupled levels (as discussed later) is mostly referred to as Δ, FIR (Fluorescence Intensity Ratio), or LIR (Luminescence Intensity Ratio), depending on the authors.[17,24,33,34] In this article we will refer to it as the Δ-parameter. It is usually calculated with respect to the integrated areas under the peak. If peaks overlap, or they exhibit complicated splitting, it is also possible to use the intensities of the peak maxima (Eq.1).[17,24]

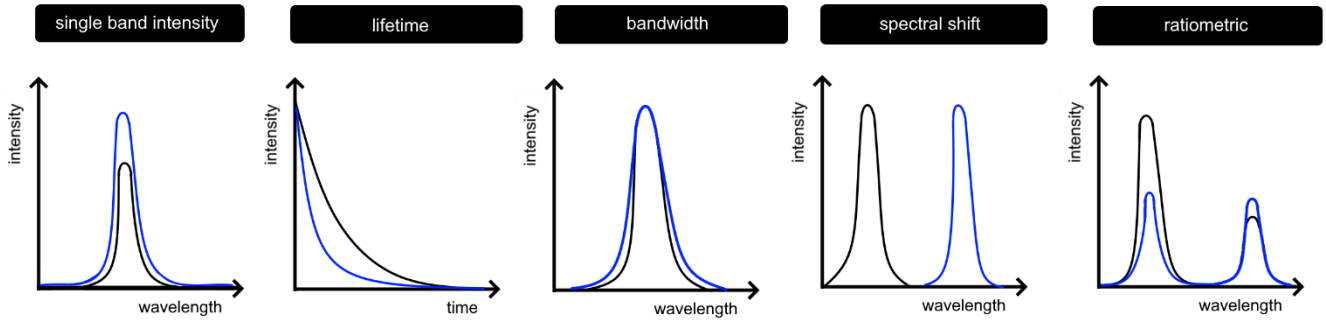

Figure 3 Types of read-outs for nanothermometry: single band intensity, lifetime, bandwidth, and spectral shift-based, as well as ratiometric readout type. The blue curves represent a readout as it is expected for higher temperature, the black curves are the baseline measurements at room temperature.

$$\Delta = \frac{I_1}{I_2} \quad (1)$$

Important performance parameters that are based on *Δ* are the relative sensitivity S_r, temperature uncertainty, and the temperature resolution.[17]

The relative sensitivity, S_r is defined as the change of *Δ* with a change in temperature normalized with regards to *Δ* (Eq.2), with *T* being the temperature.

$$S_r = 100\% \times \left|\frac{1}{\Delta}\frac{\partial \Delta}{\partial T}\right| = 100\% \times \frac{\Delta E}{k_B T^2} \quad (2)$$

If thermally coupled levels are used (explained later in detail), this equation can also be expressed with the energy difference between the thermally coupled levels *ΔE* and the Boltzmann constant k_B, as shown on the right side of the equation. The relative sensitivity does not depend on the quantity of material measured and can therefore be used to compare different materials and studies.[17,24]

The uncertainty, δT describes the trueness of the measured value compared to the actual physical value that is measured (Eq.3). The temperature resolution describes the smallest change in temperature that causes a measurable change in *Δ*.

Other important performance parameters are reproducibility and cycling stability.[17] Reproducibility describes how accurately the result can be replicated, while cycling stability describes how often a result can be reproduced before the material degrades.

$$\delta T = \frac{1}{S_r}\frac{\delta \Delta}{\Delta} \quad (3)$$

To improve the thermometric performance also other atoms can be co-doped into the Ln^{3+}-doped matrixes.[26,35] These atoms can be *d*-block transition metal ions like Ti^{2+}, V^{2+}, Cr^{4+}, Mn^{4+}, Fe^{2+}, Co^{2+}, Ni^{2+}, Cu^{2+}, and Mo^{3+},[17,26,35] or alkali ions like Na^+, Li^+, K^+, Ca^{2+}, Sr^{2+}.[29,36] In both cases, the increased asymmetry of the crystal leads to improved and/or tuned photoluminescence. Energy transfer between the ions often also occurs in co-doped lanthanide-transition metal ion compounds. Some of these systems can operate as lanthanide-sensitized transition metal UC or transition metal sensitized lanthanide UC.[17] Using lanthanides as sensitizers typically involve Yb^{3+} as a sensitizer and $Mn^{3+/4+}$ or Cr^{3+} as an activator. Introduced into the solid material, transition metal ions offer incompletely filled *d*-shells and provide energy levels as well as a strong interaction of the crystal field with the surrounding *3d*-orbitals.[17] Their electronic configurations allow electronic transitions that are parity-allowed, unlike the *4f-4f* ones from the lanthanides that are *La Porte* forbidden. That intrinsic feature results in intense and broad absorption and emission bands, which are mostly more temperature-dependent than lanthanides. Another feature is that *d*-metal ion co-doping is known to affect the ratio of green-to-red emission in UC for Yb^{3+}-Er^{3+} systems. They alter the energy transfer processes to the lanthanide ions and improve the thermometric performance of the nanothermometer.[17,26,35]

Ratiometric thermometry suffers severely if the intensity of the emitted radiation decreases, leading to a lower signal-to-noise ratio and larger readout error.[24,25] Different strategies for sensitization are currently investigated and developed. Achieving higher intensities leads to a lower temperature uncertainty and improved quality of the signal, therefore a better readout.

Thermally coupled levels

The population of energy levels can be thermally influenced, meaning that their population is affected by energy in form of temperature. If the thermally caused depopulation of one energy level causes the population of the other energy level, the energy levels are called thermally coupled. Boltzmann ratiometric thermometry is based on the intensity ratio of two thermally coupled levels.[24,25,29,37] The thermometric parameter *Δ* is defined as the ratio of the thermally coupled levels. The population of the excited energy levels can be described with the Boltzmann distribution (Eq.4). This distribution is commonly used for upconversion systems. The absolute temperature is inversely related to the logarithm of the thermometric parameter. The energy difference between those thermally coupled energy levels is called *ΔE*.

$$\Delta = \alpha * e^{\frac{-\Delta E}{k_B T}} \quad (4)$$

Materials exploited for nanothermometry

Up to date, various materials and material-combinations have been used for developing nanothermometers.

Quantum dots (QD) are semiconductor nanoparticles like PbS, CdSe, CdSeTe, CuS, Cu_2S, $CuInS_2$. In biomedical applications, they can be used as nanothermometers, but also as sensitizers in combination with e.g., Ln^{3+}-doped nanoparticles.[24,25,38] However, QDs are not ideal for biological applications because they are excited in the UV or visible region, leading to limited tissue penetration and strong background signal.[25] In addition, QDs offer only a limited efficiency due to their non-linear process, making pulsed laser excitation necessary.[25] This makes the application of QDs very expensive. A general shortcoming is that most QDs show toxic behavior *in vitro*,[38,39] e.g., for CdSe. An exception is Ag_2S, which does not exhibit highly toxic behavior, and is currently being extensively explored by some research groups.[40,41] A major drawback is the low development maturity for non- or less toxic QDs for biomedical applications.[38,39] Self-purification is another commonly known issue when working with QDs.[42]

Lanthanide-doped upconversion nanoparticles (UCNPs) are guest-host systems where trivalent lanthanides are doped in an appropriate dielectric host lattice.[17,25,29] They are less than 100 nm in size, but for biomedical applications, size of less than 30 nm is commonly desired.[25,31] The Ln^{3+}-dopants are the optically active centers that produce emissions after excitation with an appropriate wavelength. Depending on the used lanthanides, the emission wavelength can be tuned readily,[25,29,42] thereby color tuning of selected upconversion and downshifting can be achieved. Most commonly Vis (blue, green, red) and UV emissions are achieved with lanthanide UCNPs. It is also

possible to achieve NIR-to-NIR UC systems, but far less common.[43] The photoluminescence of the Ln^{3+} arises from the *4f-4f* electronic transitions within one ion.[30,31,44] These are *La Porte* forbidden, however, the quantummechanical selection rule is only relaxed due to crystal field intermixing.[45,46] Their forbidden nature leads to very weak emission intensity but also a long lifetime of excited states.[24,25,44] Another characteristic feature of lanthanide ions are their very sharp line emissions that are resistant to photobleaching[25,45] and photoblinking.[25] These features are caused through the shielding of the *4f*-orbitals by the fully filled outer *5s* and *5p* orbitals.[24,25] Ln^{3+} UCNPs are suitable for single band intensity, ratiometric, and lifetime thermometry. For Ln^{3+} UCNPs a spectral shift or bandwidth change with temperature is not significant and is not used for nanothermometry.[24] Other important intrinsic attributes are high chemical stability, good repeatability, the possibility of NIR-light excitation and color tuning, and large anti-Stokes shifts.[17,25] All the above-mentioned features make them promising systems for biomedical applications.

Ln^{3+}, Yb^{3+} co-doped systems (where Ln^{3+} = Tm^{3+}, Ho^{3+}, Er^{3+}) usually work with energy transfer upconversion (ETUC) where Yb^{3+} absorbs NIR light and gets excited from its ground $^2F_{7/2}$ state to its first excited state $^2F_{5/2}$.[31] The absorbed energy is then transferred to adjacent Ln^{3+} ions such as Tm^{3+}/Ho^{3+}/Er^{3+}. In the case of Er^{3+}, the energy is transferred to the $^2H_{9/2}$, $^2H_{11/2}$, $^4S_{3/2}$, and $^4F_{9/2}$ energy levels, generating violet emission at a wavelength of 415 nm ($^2H_{9/2} \rightarrow {}^4I_{15/2}$), green emission at 525 nm ($^2H_{11/2} \rightarrow {}^4I_{15/2}$) and 540 nm ($^4S_{3/2} \rightarrow {}^4I_{15/2}$) and red emission at 655 nm ($^4F_{9/2} \rightarrow {}^4I_{15/2}$). In the case of Ho^{3+}, upconversion emission occurs from the $^5F_4$, $^5S_2 \rightarrow {}^5I_8$ energy transition (green at 545 nm), the $^5F_5 \rightarrow {}^5I_8$ (red at 650 nm) energy transition, and the 485 nm, $^5F_3 \rightarrow {}^5I_8$ (blue at 485 nm) energy transition. Compared to the Er^{3+}-Yb^{3+} pair, the Ho^{3+}-Yb^{3+} pair has a poor energy level match, leading to a lower upconversion efficiency.[31] Upconversion emission from the Tm^{3+}-Yb^{3+} pair arises from the $^3H_4 \rightarrow {}^3H_6$ energy transition (NIR, 800 nm), the $^3F_3 \rightarrow {}^3H_6$ (red, 695 nm), the $^1G_4 \rightarrow {}^3F_4$ (red, 645 nm), the $^1G_4 \rightarrow {}^3H_6$ (blue, 475 nm), the $^1D_2 \rightarrow {}^3F_4$ (blue, 450 nm) and the UV emissions at 365 nm ($^1D_2 \rightarrow {}^3H_6$), 645 nm ($^1I_6 \rightarrow {}^3F_4$) and 290 nm ($^1I_6 \rightarrow {}^3H_6$). Tm^{3+} offers minimized non-radiative relaxations and little cross relaxations within the activator.[28]

Host materials for lanthanide-doped upconversion nanoparticles (UCNPs)

The selection of an appropriate host material is essential for highly efficient upconversion as it affects both the phonon dynamics and the local crystal field.[25,28] A low phonon cut-off energy and a low crystal field symmetry are generally desirable. Host materials should be optically transparent, have a low probability of optical damage and high chemical stability. Non-radiative losses in UC are mainly induced by phonons as the process is sensitive to the phonon density of states.[25] Multiphonon-assisted relaxations are a major factor in low luminescence efficiency. These relaxations cause the excited state to relax with the conversion of the absorbed energy into lattice phonons and therefore without emission. The number of phonons needed for multiphonon-assisted relaxation defines the phonon cut-off energy. A larger number of phonons needed to convert the excitation energy into phonons correlates with a lower efficiency of the nonradiative process, hence a low phonon cut-off energy in a dielectric host is desired.[25] Collective oscillation of electrons at a metallic interface is called localized surface plasmon resonance (LSPR). It is caused by the electromagnetic interaction of metal and incident light if the distance between the fluorophore and the metal is appropriate. LSPR is utilized to enhance the PL from dyes or QDs.[25]

The crystal field provided by the host material affects the UC efficiency of the Ln^{3+} active centers to a great extent.[25,28,47,48] Its local crystal symmetry strongly influences the optical properties of the emitters as it affects the ion-to-ion distance, spatial arrangement, and the coordination number of the active center.[28] A less symmetric crystal phase favors intermixing of the *f*-orbitals with higher electronic configurations and partially allows the generally parity-forbidden intra-*4f*-electronic transitions, resulting in an increased UC efficiency.[25,28,48,49] This was shown e.g., in a detailed comparison of cubic and hexagonal phase $NaYF_4$ by *Klier & Kumke*.[50] The highly symmetric cubic phase showed lower UC intensity than the hexagonal phase with its higher symmetry with no change in the ratio of the peaks, as expected.[25,28] Another way to tailor the crystal field is to dope non-emitting ions into the crystal to change its symmetry.[25,28] This was shown for e.g., by *Wang et al.* with the incorporation of different amounts of Gd^{3+} in Er^{3+},Yb^{3+}:$NaYF_4$.[48] They showed that the phase and size of the nanoparticles could be controlled precisely, and the UC intensity varied depending on the doping concentration. They attributed the respective increase of intensity to an increase in hexagonal crystal phase. However, it was proposed that the ion incorporated into the crystal lattice might also quench the luminescence due to efficient energy transfer to e.g., Sm^{3+} and Nd^{3+}, therefore the proper choice of ion is important. The ion must be of appropriate size for the host lattice and offer a simple energy structure with energy levels sufficiently far away from each other. Also, core-shell structures (as discussed below) introduce distortions of the crystal symmetry. Both variations lead to a less symmetrical crystal, increasing the UC efficiency as described above.

Fluorides as host matrix for lanthanide doping are the most widely used materials due to their well-established synthesis and widely researched structure. Commonly used fluorides are CaF_2, $NaGdF_3$, $NaLuF_4$, $NaYbF_4$, LaF_3, $LiLuF_4$, YF_3, but also more exotic materials such as $BaYF_5$, $KMnF_3$, KLu_2F_7, K_3YF_6, KYb_2F_7, $LiLu_2F_7$, Li_4ZrF_8, $NaBiF_4$, $NaYb_2F_7$, SrF_2, Sr_2GdF_7, Sr_2LuF_7, Sr_2YF_7, Sr_2YbF_7 have been explored.[29] Their application and performance depend on the temperature range and emitting ion(s) used. This class of materials offers high refractive indices, chemical inertness, strong thermal stability, low non-radiative decay rates, high radiative decay rates, high ionicity, large band gaps, high luminescence quantum yield, long lifetimes, and the lowest phonon cut-off energy compared to other materials common for upconversion, e.g., 350 cm^{-1} for $NaYF_4$.[25,29] They are used in both downshifting and upconversion systems. Additionally in combination with Ln^{3+} ions they offer high ionicities and coordination numbers, resulting in low vibrational

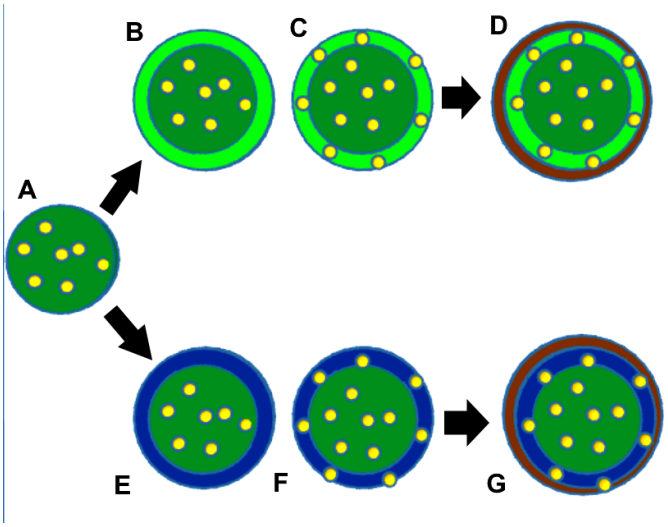

Figure 4 Commonly used core-shell approaches: a doped core (left) is shelled with an (un)doped shell of the same (upper route) or different (lower route) material. If a doped shell is chosen, an inert shell can be grown around the core-shell particle. The core-shell-shell particle is shown on the right with both core-shell combinations.

energies.[29] Well-established routes like co-precipitation and solvo- or hydrothermal synthesis in an autoclave or a Schlenk line yield particles of various shapes and sizes that can also be fine-tuned.[17]

Besides fluorides, other material classes can be used for designing UCNPs, namely orthophosphates, vanadates, oxides, oxysulfides, and oxyfluorides/-sulfites. Lanthanide orthophosphates like $LnPO_4$ are known for their high chemical, thermal and mechanical stability and are widely utilized in different applications.[29] In addition, $LnPO_4$ offer a great refractive index and a very high phonon cut-off energy of 1100 cm^{-1}.[29] The material class is known for its highly efficient energy transfer, spectral color purity, and abundant shape possibility. Lanthanide orthovanadates such as $GdVO_4$, YVO_4 and $LuVO_4$ are well studied and offer highly efficient energy transfer, spectral color purity, high thermal stability, and a wide and extreme UV absorption.[29] Vanadates usually possess comparably high phonon energy (e.g., YVO_4 has a phonon cut-off energy of 890 cm^{-1}).[17] Metal molybdates with a $MMoO_4$ structure (where M = Ca, Sr, Ba) can be sensitized with lanthanide ions and offer high refractive indexes, low phonon threshold energy of around 850 cm^{-1}, and robust chemical and physical properties.[29] Oxides have comparably low phonon energies (e.g. Y_2O_3 has a phonon cut-off energy of 550 cm^{-1} and ZrO_2 has 500 cm^{-1}).[25] Oxysulfides like Y_2O_2S and oxyfluorides/-sulfites like GdOCl demonstrate comparable phonon cut-off energies (520 cm^{-1} for Y_2O_2S and 500 cm^{-1} for GdOCl).[25] Regular particles in the correct (nano)size can be challenging to synthesize, depending on the material. Especially for vanadates, synthesizing regular nanoparticles is associated with a lot of effort. Many of these materials have not been researched sufficiently and are less optimized compared to fluoride host materials, so fine-tuning of their morphology is still challenging.

Shelling / core-shell structure

Shelling core nanoparticles with an inert or an active shell is a common approach for UCNPs to improve their photoluminescence intensity.[24,25,31,50,51,52] There is a large variety of core-shell combinations, the most common ones have been overviewed in Fig.4. The core (A) and shell can be composed of the same material, as shown in the upper route (B and C). The shell can be either doped itself (C) or remain undoped (B). Another approach is to grow a shell of a different material around the core (E and F). These shells can also be doped (F) or undoped (E). More complicated structures can be grown with different doping ions or core/core-shell of different material, as indicated by the last particle core-shell-shell structure in both rows (D and G). These shells can be made of the same or different material as the core/core-shell and/or the shell.

If the shell is doped with one or more luminescent ions, it is called "active" as it can emit photoluminescence.[24,25,31,52] It has been shown that very complicated core-shell structures with sophisticated interplay can be grown. These can be used for different applications and are usually fine-tuned to cater to various needs. An example of multi-shelling was reported for $NaYF_4$@$NaGd_{0.8}Er_{0.02}Yb_{0.18}F_4$@$NaGd_{0.75}Nd_{0.25}F_4$ by *Ferreira et al.*[53] The differently doped shells were investigated via STEM EDX mapping, showing the sophisticated structure. Another approach is the so-called "sandwich" structures, where an activator and a sensitizer are grown separately in a shell-like structure as was shown by *Dou et al.* for Er,Yb:$NaYF_4$@Er:$NaYbF_4$@Tm,Yb:$NaYF_4$.[54] Active core-active shell Er^{3+},Yb^{3+}:$NaGdF_4$@Yb^{3+}:$NaGdF_4$ particles were synthesized and compared to their active core-inert shell counterparts by *Vetrone et al.*[55]

A core-shell structure is known to eliminate quenching by the surroundings as it provides an inert shell between the doped core and the solvent.[24,25,31,52] The shell can be made of the same or a different material than the core. Commonly used and well investigated material combinations are $NaYF_4$@$NaYF_4$ and $NaYF_4$@$NaGdF_4$.[51,52,53] Although not well investigated in the literature, especially if the core and shell of the particle are made of the same materials, ion migration can be an issue. The issue of ion migration was observed by *Kaczmarek et al.* in cube and diamond-shaped core-shell Er^{3+},Yb^{3+}:$LiLuF_4$@$LiLuF_4$ nanoparticles via STEM EDX mapping and further confirmed through high-temperature luminescence measurements in air and nitrogen atmosphere.[56] It was observed that the emissive dopants did not retain in the core but migrated to the surface of the core-shell particle. The shell was no longer inert, and the photoluminescence was quenched as the medium molecules could couple with the lanthanide ions present on the surface of the nanoparticles. However, other material combinations, such as Er^{3+},Yb^{3+}:$NaYF_4$@$NaYF_4$ do not show this kind of behavior, as shown by *Ferreira et al.* on very sophisticated multi-shell particles.[53] Ion migration is, without a doubt, an issue that is not investigated thoroughly. Many researchers are not aware of its possibility or do not carry out sufficient material characterizations.

(Organo) silica shell

Coating nanoparticles with a silica layer circumvents prominent issues such as toxicity, quenching from solvents, and water-solubility; and offers the possibility of functionalization, which is necessary for many biological applications.[25,38] The silanization can be carried out on both hydrophobic and hydrophilic nanoparticles employing different methods.[25] For hydrophilic NPs, the Stöber process is the most exploited, where TEOS (tetraethoxysilane) is added as the coating precursor. With this method, very thin and homogenous coatings can be achieved as demonstrated by *Li et al.* with their adjustable layer thickness of 1-3 nm on $NaYF_4$ NPs.[57] The reverse-micelle reactor method produces thin layers on hydrophilic nanoparticles using a surfactant such as Igepal in combination with TEOS as a precursor.[25] In both methods it is possible to use a mixture of e.g., TEOS and APTES (3-aminopropyltriethoxysilan) to obtain a mesoporous silica coating that offers functionalization.[25] Functionalization is a vital part for theranostics and other biomedical and biological applications as it offers to adjust to the specific needs of e.g., drug release in cells.[25,38,58] For example a mesoporous silica shell was grown around core-shell Er^{3+},Yb^{3+}:$NaYF_4$@$NaYbF_4$ by *Lv et al.* as a platform for theranostics, namely for dual-mode upconversion, photoacoustic imaging, and photothermal imaging.[59] *Zhao et al.* grew yolk-shell nanocages for photo-regulated drug release, combining Tm^{3+},Yb^{3+}:$NaYF_4$@$NaLuF_4$ UCNPs as yolk with a mesoporous silica shell of 10 nm thickness.[58] This combination allowed for a sophisticated platform with the potential to be used in theranostics.

5. Shortcomings of luminescence nanothermometry

UCNPs are susceptible to photoexcitation intensity and different operation modes like continuous wave or pulsed laser operation.[24] Another common issue is the self-absorption of the emission previously emitted by the nanothermometer as well as reabsorption. Autofluorescence of biological tissues is also a major drawback as the spectral overlap of the medium (fluorophores) and the nanothermometers affects the signal readout.[24] All of the before mentioned issues may diminish the quantum yield or create artifacts influencing accurate temperature readouts. Also, factors other than temperature affect the calibration curve, the brightness, operation range, and resolution, but are rarely studied. The excitation energy also influences the measurements, especially at very high laser powers as the population cannot be described with the Boltzmann law anymore.

Influence of surrounding medium (e.g. solvents)

The absolute intensity does not only depend on the temperature but is also highly influenced by the local concentration of the nanothermometers, the illumination intensity, and the inherent properties of the tissue.[24] The physical and (bio)chemical environment, namely pH value, viscosity, solvent medium, and ligands, all influence the intensity greatly.[24,60] Particularly for *in vitro* and *in vivo* imaging this is of great importance as these parameters vary heavily and therefore lead to wrong thermal readouts and/or artifacts. This is especially problematic when already significant instrumental artifacts are present. Ln^{3+}-doped nanoparticles are generally more resistant to the influences of their surrounding medium but are not unaffected. Their quantum yield, lifetime, and spectral distribution have shown to vary with a change in solvent, pH, or medium polarizability.[24] Water and tissue have extinction coefficients that are strongly dependent on the incident wavelength. Water absorbs strongly around 980, 1150, and 1500 nm, which has led to defining the so-called biological windows (Fig.5).[17,24] The first biological window (BW-I) refers to the range from 650-950 nm, BW-II is represented by the range from 1000-1350 nm, and the third biological window (BW-III) ranges from 1550-1850 nm of the spectral region. These regions offer the advantage of weak water absorption and are therefore favorable for nanothermometry meant for biological purposes. Tissue scattering becomes more dominant for absorption wavelengths shorter than 650 nm, making tissue absorption highly dependent on the wavelength.[24] Another issue related to tissue is spontaneous emission from endogenous fluorophores and self-absorption. Nanothermometers operating in the BW-II are significantly influenced by this due to the strong and

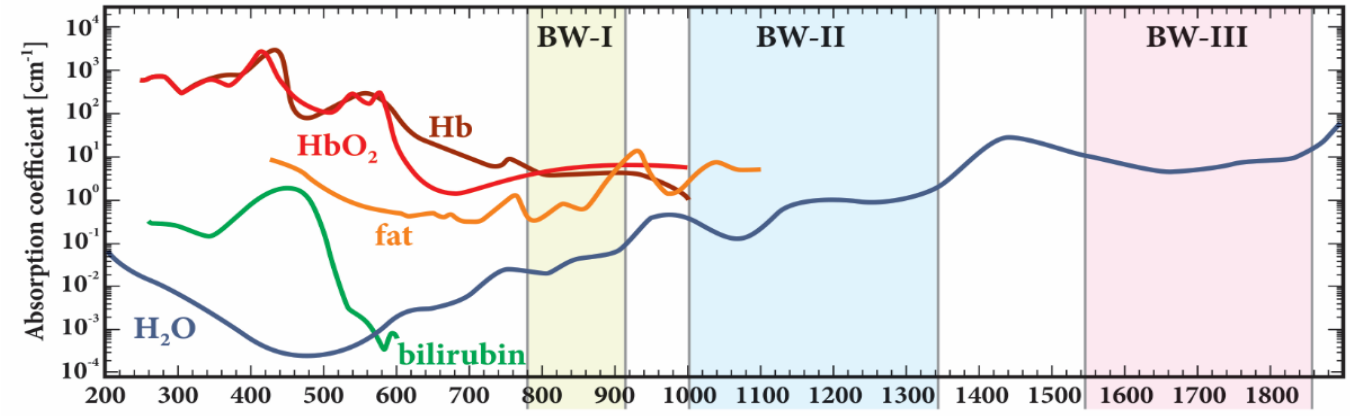

Figure 5 Dependence plot of absorption coefficients of some major tissue components on wavelength spanning over the three biological windows. Reproduced from Reference [17], with permission from Elsevier.

increasing water absorption. Spectroscopic features caused by either water or tissue absorption can cause significant change of the spectrum.

Thermal quenching and concentration quenching

Most nanothermometers have a negative thermal coefficient, meaning that the brightness decreases with increasing temperature. This can be troublesome as it decreases the signal-to-noise ratio and possibly leads to inaccurate read-outs.[24]

Cross relaxation (CR) is readily introduced with a higher doping concentration of activators as the average distance between the doped ions decreases, leading to deleterious energy transfer and migration.[25] Sensitizer ions are usually not able to introduce CR as they have a much simpler energy level structure, nevertheless, an increased doping percentage does lead to quenching.[25] It is believed that quenching effects by sensitizer ions are caused by energy migration to quenching sites in the sublattice. The exact percentage of doping varies heavily with the choice of system and host.

Influence of particle surface and ligands

It is important to note that nanoparticles emit much weaker luminescence compared to bulk materials, due to their small size while retaining their spectral features.[47] This is called the surface quenching effect. Another inherent issue is the high surface-to-volume ratio,[25,47] increasing the surface defect density with decreasing particle size. This also contributes to a suppressed UC intensity. Surface-induced deactivation can be either caused by dopants at or around the surface or by energy migration.[25] In the former case dopants on the surface are deactivated by neighboring surface quenching centers. In the latter case, the energy absorbed by dopants in the center of the particle is migrating randomly and can travel long distances to the surface quenching sites. UCNPs must be able to be surface-engineered and their ligands must be bio-functionalizable. For biological applications, especially theranostics, the aim is usually to combine different functionalities in one platform.[25,30,32] As-synthesized, the nanoparticles are usually capped with long-chain hydrophobic ligands like oleic acid. These can be exchanged with other ligands, removed, altered, and so forth in order to tune the functionalities appropriately.

Toxicity

The analysis of toxicity for UCNPs meant for biological applications usually includes basic toxicity and biodistribution analysis, however, the integrity of the particles, as well as their stability in biological media and long-term accumulation is not investigated.[31,39] An interesting class of materials are biodegradable materials such as K_3ZrF_7 that can be decomposed in the human body and are therefore does not accumulate in organs, posing the risk of toxicity.[28,32] The toxicity can be evaluated both *in vitro* and *in vivo*.[31] The most convenient approach is cell viability tests where nanoparticles are brought in contact with cultured cells to evaluate their (non)toxicity. Other *in vitro* approaches are cell proliferation and differentiation, where the nanoparticles influence the ability of cells to differentiate and proliferate, and hemolysis, where the nanoparticle is investigated in terms of its ability to cause hemolysis.[31] *In vivo* tests are carried out in different organisms such as *C. Elegans,* zebrafish, mice, and rats.

Excitation @980 nm and heating in BWI/II

UCNPs are mostly excited with a 980 nm laser, whose energy is absorbed by Yb^{3+} ions in the system. Yet, excitation with a 980 nm wavelength induces heating.[24,25] The strong absorption of tissue and water is the reason for the increasing temperature, leading to damaged tissue and/or wrong readout temperatures. A solution to overcome this issue would be to shift to slightly different wavelengths (e.g., 940 nm or 950 nm), that still sufficiently excites into the Yb^{3+} band but causes less to no heating.[24,25,61,62,63] Another solution is to shift the excitation wavelength with a second sensitizer, e.g., Nd^{3+}.[61,62] This way the second sensitizer is excited and can transfer its energy to Yb^{3+} and the excitation wavelength can be shifted to 800 nm. A different approach is using dyes to shift the excitation wavelength as it was proposed by *Chen et al.* for UCNP@BSA-RB-IR825 theranostic nanoparticles that were excited at 808 nm.[63] *Zhan et al.* presented 2% Tm^{3+}/Er^{3+}/Ho^{3+}-doped $NaYbF_4$ UCNPs for *in vitro* and *in vivo* bioimaging using 915 nm excitation, circumventing the issue of tissue overheating.[64] Their UCNPs could be heated for significantly longer periods of time, which was proven experimentally and computationally. Additionally, the penetration depth of the 915 nm CW excitation is deeper, which was shown both *in vitro* and *in vivo*.

6. Hybrid materials with UC systems for biological thermometry

Developing hybrid materials can be a challenging task. Combining hybrid organic-inorganic materials with Ln^{3+} ions allows to overcome the issue of the small absorption coefficient of the lanthanides as they offer the above-described antenna effect of the ligand and subsequent sensitization. This is relevant for downshifting luminescence systems and in some cases can also be applied for UC systems.

Dye-sensitized hybrid materials, such as the SiO_2-coated dye-sensitized $NaGdF_4$ reported by *Zhou et al.*, can be developed.[65] Most UC hybrid systems utilizing dyes rely on the Förster Resonance Energy Transfer (FRET) mechanism where a fluorescence donor is quenched by an acceptor, and fluorescence emission is therefore enhanced.[66] This mechanism might be expanded into a fluorescent FRET network where donors and acceptors are incorporated connected into a network. FRET is linearly dependent on the distance between acceptor and donor and therefore also on the concentration of both in the upconversion material. As photostability and photobleaching are an issue, SiO_2-coating can be a good solution to increase the robustness of the hybrid material. In general, an issue for biomedical applications is phototoxicity.[66] Due to incident UV light the formerly little to non-toxic compound becomes toxic and actively harms the organism. This issue can be circumvented by using NIR light as incident light.

However, it has to be kept in mind that currently the state-of-the-art is using UV-Vis light.

A bottleneck in the development of dye-sensitized UC hybrid materials is that most dyes absorb around 800 nm, which is a bad energy match with Yb^{3+} as a sensitizer.[67] Due to this low spectral overlap energy transfer from the dye-antenna to the sensitizer is inefficient. A common approach to overcome this limitation is to add Nd^{3+} as a second sensitizer into the material to improve the energy match and therefore efficiency of energy transfer from the antenna to Yb^{3+} and activator ion.[66,67,68] Additionally, the absorption cross-section of Nd^{3+} is significantly larger than that of Yb^{3+} with an energy transfer that is considered to be efficient.[69] However additional Nd^{3+} doping holds the issue of energy back transfer from the activator into Nd^{3+} energy levels, leading to emission quenching.[69,70] Efficient energy transfer is not only in need of sufficient spectral overlap but also sufficient physical distance between dye molecules and Ln^{3+} ions.[68] Shortening this distance however remains a challenge to-date because the addition of too many dye molecules on the surface of the hybrid particle might lead to energy aggregation and consequent energy back transfer, resulting in emission quenching.[66,68] This can especially be an issue if the core or core-shell particle is silica-coated with a coating thickness that does not allow energy transfer from the dye to the sensitizer.[66]

Zou et al. significantly enhanced the emission intensity of their $NaYF_4$:Er,Yb nanoparticles with sensitization with IR-806.[67] *Xu et al.* presented their $NaGdF_4$:Yb,Er@$NaGdF_4$:Nd,Yb IR-808 sensitized and silica-coated nanoparticles for photodynamic therapy and bioimaging.[69] The silica was loaded with dual-photosensitizers Ce6 and MC540 and IR-808 and therefore provides a tri-modal imaging platform. *Wei et al.* were able to shift the onset of concentration quenching in Nd^{3+}:$NaYF_4$ from 2-20 % Nd^{3+} due to sensitization with ICG dye and increased the UC emission brightness by the factor of 10.[70]

Metal Organic Frameworks (MOFs) are periodic 3D porous networks with inorganic nodes and inorganic linkers.[71] These clusters or linkers themselves can introduce luminescent features or properties and can offer the incorporation of specific organic compounds and/or molecules into the framework.[72] They integrate the advantages of both organic and inorganic materials, giving rise to interesting opportunities. An important feature of this class of materials is their inherent stability of the structure.[72]. Among MOFs, Zr-based MOFs are the most water-stable with intrinsically high chemical stability, which makes them well-suited for biological applications. Ln^{3+}-doped MOFs are explored especially in the context of drug delivery with the MOF offering opportunity for drug loading and releasing with its porous structure.[66] Ln^{3+}-doped MOFs have been studied extensively for downshifting.[71,72,73] *Li et al.* reported that tunable UC emission can also be achieved by varying the ratio of Ln^{3+} in the MOFs as it was demonstrated for a series of Ln^{3+}-based Er^{3+},Yb^{3+} doped Y^{3+}-MOF.[72] In this way, excitation in the NIR region/BW-I and emission in the BW-II is obtained, which is vital for biological applications, as discussed earlier.[64] MOFs can be used to develop hybrid UC nanocomposites.[65,75,76] *Rijckaert et al.* reported the hybrid $NaYF_4$:Er^{3+},Yb^{3+}@NaYF4@nano-MOF@AuNPs@LB composite (Fig.6), that they utilized for nanothermometry in water in the physiological range.[77] UiO-66-NH_2 was used as the MOF, offering a high surface area due to its mesoporosity. The lipid bilayer (LB) wrapped around the nano-MOF improved biocompatibility. They showed that this nano-MOF was able to accommodate not only $NaYF_4$:Er^{3+},Yb^{3+}@$NaYF_4$ UCNPs but also AuNPs, making it a proof of concept to work as a platform for both nanothermometry and plasmon-induced hyperthermia.

Covalent Organic Frameworks (COFs) are advanced porous crystalline materials with strong covalent linkages that have recently been shown to work as platforms for grafting lanthanide ions, but can also be grown as shells around UCNPs.[78-81] COFs are composed of light elements such as boron, carbon, nitrogen, oxygen, and silicon, and offer large surface area, structural versatility, effortless surface modification, and high chemical and thermal stability.[78] Unlike MOFs, they offer reasonable crystallinity and long-range ordered structure with reversible synthesis methods as condensation reactions with properly chosen 2D or 3D organic precursors.[71,78] Up to date,

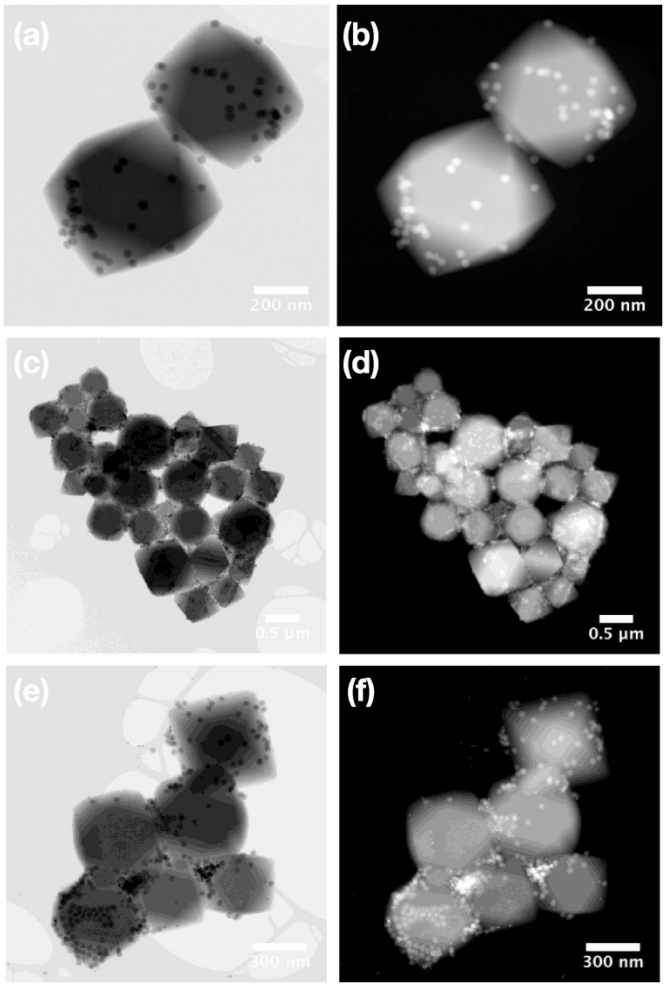

Figure 6 (S)TEM images of (a), (b) β-$NaYF_4$:Er,Yb@β-$NaYF_4$@nano-MOF, and (c)–(f) β-$NaYF_4$:Er,Yb@β-NaYF4@nano-MOF@AuNPs. Reproduced from Reference [77], with permission from Elsevier.

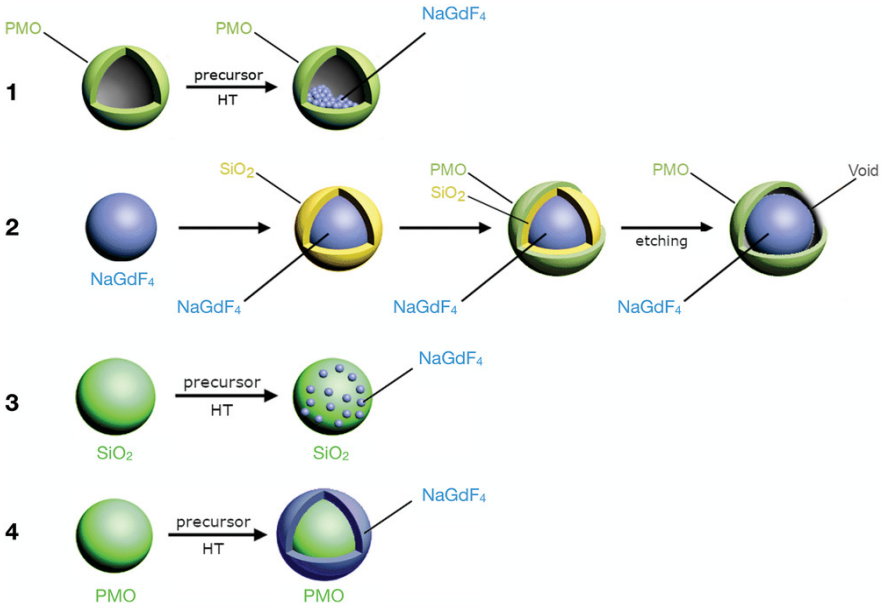

Figure 7 Schematic illustration for the preparation of four hybrid PMO/mSiO_2-inorganic materials. Reproduced from Reference [86], with permission from John Wiley and Sons.

COFs and COF-based hybrid materials have not been extensively explored for nanothermometry. However, their great adjustability of properties combined with their inherent chemical and thermal stability is promising and already widely explored in catalytic applications, as well as stable platforms for photoredox reactions.[78]

Periodic Mesoporous Organosilicas (PMOs) are hybrid organic/inorganic porous materials obtained through a sol-gel process from a silsesquioxane as an organic precursor with the help of a surfactant working as a soft template. Porous PMOs offer functional groups not only at the surface, but also in the PMO walls and therefore strongly influence the flexibility or rigidity of it and the general structure. They offer a large variety of functional groups, morphology, and tuning of mesoporosity and exhibit advantageous long-term hydrothermal, (bio)chemical, and mechanical stability.[71] Light-emitting PMOs, especially lanthanide-grafted ones, are a relatively new but in recent years more frequently explored option, as described by *Kaczmarek et al.* in their 2020 review.[82] PMOs can be emissive on their own due to fluorescent organic groups on the surface and/or pore walls that offer light emission. They can also accommodate emissive ions into their pores.[70,82] Crucial for luminescence in biological applications, especially drug delivery, is that PMOs can be obtained both in nanosize and as hollow materials with pores that can be easily loaded. Most up-to-date developed Ln^{3+}-PMOs are downshifting systems, comprising e.g., Eu^{3+} and Tb^{3+} or Sm^{3+} and Tb^{3+}. Such materials have been explored as nanothermometers for biological applications.[79,83,84,85] Hybrid PMO-inorganic materials can also become very attractive for developing UC systems. In 2020, *Kaczmarek et al.* presented a hybrid PMO structure composed of Er^{3+},Yb^{3+}-doped β-$NaGdF_4$, and PMO/mesoporous silica (mSiO_2) for Vis and NIR UC with potential for *in vivo* nanothermometry.[86] Four different hybrid materials were prepared (Fig.7). Two nanorattle structures were developed, where in the first a hollow PMO was loaded with Er^{3+},Yb^{3+}:$NaGdF_4$. In the second approach, a PMO shell was grown around Er^{3+},Yb^{3+}:$NaGdF_4$ NPs with a void in-between the NPs and PMO layer. Also, mSiO_2 loaded with Er^{3+},Yb^{3+}:$NaGdF_4$ NPs and PMO shelled by a Er^{3+},Yb^{3+}:$NaGdF_4$ layer were reported in this work. PMOs offer the benefit of being degradable All hybrid materials showed no toxicity in *in vitro* cell viability tests, only at very high concentrations of 0.5 to 1 mg per well the cell survival rate dropped to 50-60 %. The low cell survival rate was attributed to the high weight of the sample at higher concentrations as NHDF cells are sensitive to mechanical pressure. The photoluminescence of all prepared materials was investigated. The nanorattle-structure of a PMO shell around Er^{3+},Yb^{3+}:$NaGdF_4$ with a void in-between showed a major improvement in performance after etching as compared to before etching. The nanothermometry of this combination showed a maximum relative sensitivity of 1.31 %/K ($^2H_{11/2}$, $^4S_{3/2}$ → $^4I_{15/2}$) or 0.7 %/K ($^2H_{11/2}$, $^4S_{3/2}$ → $^4I_{13/2}$) at 293 K with an uncertainty smaller than ±1 K and a repeatability of 97-98%.

7. Theranostics

Theranostics is a term coined from the words **thera**py and diag**nostics** and refers to the relatively young, but multifaceted research field in clinical (nano)medicine uniting specifically targeted therapy methods with innovative diagnostic approaches via single, but multimodal nanovehicles/nanoplatforms that offer a bio-functionalization platform for drug loading and specific delivery to targeted organs, tissues, and even individual cells.[87,88] Many thermoresponsive drug delivery systems combining at least two exploitable physicochemical properties have been introduced for such purposes,[89] but no ideal nanoagent for universal diagnosis and therapy of various clinically differing diseases and conditions has been so far developed. Such nanomaterials can

be very generally classified by their composition into metal, inorganic, carbon-based, organic, and inorganic-organic (hybrid) systems.[5,89,90] In that sense, hybrid upconversion luminescent nanomaterials, particularly the inorganic-organic porous nanoparticles based on the ratiometric luminescent response of two thermally coupled states of lanthanide ions, have been gaining increasing attention in recent years due to their unique versatile behavior. These porous nanoparticles can be designed to accommodate, contain, and transport therapeutically-(bio)active molecules or targeting moieties for detection of certain diseases, efficiently pass the intrinsic bioprotective barriers of the body (skin, air-blood, blood-brain, etc.),[5] deliver drug loads to remote and traditionally inaccessible affected sites, as well as release the specific loads triggered by internal or external stimuli,[90,91] hence fulfilling their primary intended role.

In vivo real-time monitoring of temperature in biological tissues, however, also requires scrutinous evaluation of the mutual impact and absorptive/emissive interferences between optical irradiation and the nature of the biocomponents organically found in viable tissues. Near-infrared (NIR) irradiation is applied for excitation of the luminescent temperature nanosensors due to the enhanced penetration depth and decreased scattering and absorption of the low-energy photons by tissue constituents.[17] The optical operating range for the emissivity of the various types of luminescent lanthanide-based nanothermometers is constrained to the three biological windows representing consecutive portions of the near-infrared range of the EM-spectrum. However, innately existing constituents of tissues such as water, hemoglobin, many lipids, fatty acids, proteins, etc., which otherwise have overall large absorption coefficients spanning over the whole UV-Vis-NIR region (see Fig.5), manifest a minor but not insignificant portion of their –O-H, –C-H and –N-H vibrational modes and/or overtones through absorption in this region, and as such interfere with the optical signal emitted by the nanothermometers.[17,92] Furthermore, cells and cell components also additionally scatter light.[93] Thus, the aim is to narrowly confine the nanothermometer operating window to segments where the absorptivity and scattering of these components is minimal i.e., where the tissue is as close to being optically transparent as possible to the incoming irradiation. Another important aspect largely influencing the efficiency of *in vivo* imaging is the excitation wavelength choice. Usually, in systems where Yb^{3+} ions are used for harvesting energy, 980 nm is the most appropriate choice as it corresponds to the exact energy transition used for sensitization of Yb^{3+}. However, as already described in Chapter 5, one major issue, in this case, is tissue overheating due to heating of present water molecules by vibrational energy transfer, so to eliminate tissue damage the alternative is choosing an excitation wavelength around 800 nm which will alleviate overheating and improve tissue penetration depth and resolution. In that case, Nd^{3+} ions must be co-doped into the system for an efficient sensitization.[94] On the other hand, in routine laboratory measurements of cuvette-retained samples, the 980 nm excitation wavelength may cause optical distortions and temperature variations in biological tissue and media components, so placing a thin piece of tissue directly in front of the cuvette has been introduced to avoid read-out instabilities.[95]

Even though extensive research is still imminent, especially for the systematic transition from controlled laboratory *in vitro* conditions, then on to *in vivo* animal investigations and, in due course, ideally toward clinical human studies, there has been some noteworthy theoretical and experimental progress made on the topic of hybrid upconversion nanomaterials exploited for their thermometric performance in the physiological range under NIR-irradiation. However, to be able to apply these multifunctional materials as imaging agents, sensors in diagnostics, then subsequently or simultaneously as drug-carriers for therapeutic purposes, they need to be fully characterized by their performance parameters under stable and preferably standardized operating conditions,[17,24] as well as previously proposed universal parameters and automated spectral data acquisition, handling, and analysis platforms, already introduced previously by *Kaczmarek et al*.[96] Moreover, they need to satisfy some crucial requirements (Fig.8), like structural and (photo)chemical stability and reliability, low photobleaching and photoblinking, reproducible ratiometric thermal response, high precision, resolution, and sensitivity, low-to-no cytotoxicity, biocompatibility, water-dispersibility and/or biodegradability to small, non-toxic residues that will not accumulate and retain in the vital organs such as the liver and spleen, but will be eliminated through the usual excretion routes with no detrimental side effects. Such revolutionary nanothermometers would be characterized by efficient performance in the physiological range, they could be exploited as agents for *in vivo* clinical bioimaging and diagnosis; could be functionalized as drug carriers in drug delivery, and could potentially be used as drug “capsules” in targeted thermal therapies offering steadily controlled, accurate, effective, and harmless approach in patients for theranostics.[5]

To-date, no nanomaterial has been officially approved for theranostic purposes, even though a few inorganic contenders have been subjected to clinical trials and are currently in various clinical trial stages.[97] This may partially be due to reported inconsistencies in nanomaterials design, synthesis, batch-to-batch differences, characteristic performance parameters, environment-dependent *in vivo* behavior, contrasting biosafety and biodistribution results, inability to predict their pathway once injected into the body, the uncertainty of short-term and long-term exposure, their cytotoxicity, and the possibility of byproduct formation, as well as their biodegradability and eco-friendliness in the body and the environment, respectively. Another aspect is the animal vs. human model inadequacy that is difficult to eliminate, even further, the patient-to-patient disparities when considering the ultimate clinical trials in all phases.[5,97] These, however, should by no means deter the research attempts of scientists to overcome existing shortcomings and meet rigorous conditions, but should even further accentuate the need for more systemic and all-inclusive investigations. This multidisciplinary field offers great potential for groundbreaking discoveries that will change the course of

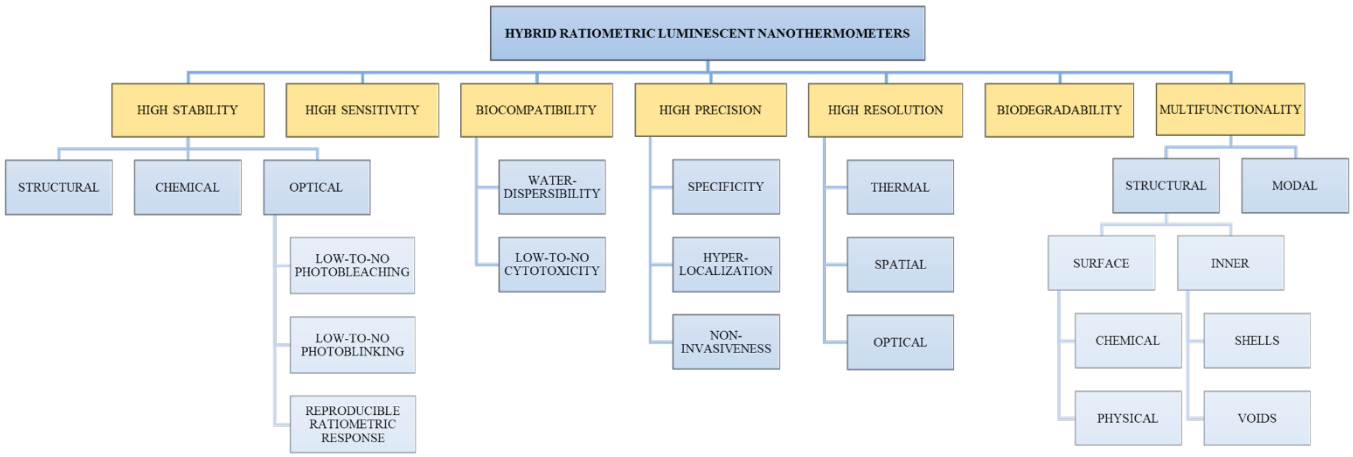

Figure 8 Diagram of most important parameters for hybrid ratiometric luminescent nanothermometers.

science and technology and will improve healthcare and the quality of life of people worldwide.

A step toward this direction in nanotheranostics has been reported recently. Namely, one of the most complex defense mechanisms of the body against toxic and pathogenic species, the so-called blood-brain barrier (BBB) represents an intricate interface between the vascular and the neural system networks. Permeating this line of defense for the purposes of drug delivery in the central nervous system is a major challenge in the field.[98] However, using low-intensity picosecond laser excitation of intravenously injected targeted AuNPs has shown effective for reversible modulation of the BBB and allowing permeation of the nanospecies delivering therapeutic cargo to the brain without damage to the neurovascular dynamics.[99] These findings pave the road for further investigations of other nanomaterials in drug delivery applications through the originally highly selective membrane by overcoming intricate bodily protective mechanisms.

With the innovative rise of the nanosciences, and in its own course, the progressive personalized nanomedicine, we envision that it is merely a question of time and looming scientific efforts and trials when nanothermometry will become a method that would be used as an equally deserving and high-performing approach, complementarily and supplementarily to all existing temperature-measurement and compatible imaging methods in clinical medicine. Research into sensing applications gives ground for the incorporation of nanothermometry within multimodal platforms for one-pot diagnosis and therapy of various diseases exhibiting significant temperature variations. Additionally, its multidisciplinary nature widens the horizon of collaborative efforts for bridging gaps between scientific fields and departments.

8. Some notable advances for *in vitro* and *in vivo* investigations of multimodal hybrid silica-based upconversion nanomaterials

There have been many noteworthy reviews of various upconversion nanomaterials reporting *in vitro* and *in vivo* nanothermometry applications published in recent years,[29,100,101,102] and even more on silica-based nanocarriers for drug delivery applications.[90,103,104,105] Hereby, we highlight the status and prospects of hybrid silica-based upconversion nanothermometers for the potential they hold towards nanotheranostics with their multifunctionality. This potential includes combination of a few modalities such as deep-tissue bioimaging, temperature sensing, photodynamic and photothermal therapy, and efficient drug delivery, all realized ideally with and within the same nanoentity.

In vitro and *in vivo* (bio)imaging

Imaging as a modality comes intuitively for upconversion luminescent nanomaterials as their optical response can be readily monitored, even though its intensity suffers from material design and tissue-dependent performance features. On the other hand, various clinical imaging methods are being applied in tumor treatment practice such as upconversion fluorescence (UCL) imaging, magnetic resonance imaging (MRI), positron emission tomography (PET), X-ray computed tomography (CT), single-photon emission computed tomography (SPECT), etc. To couple the UCL nanomaterials with existing biomedical imaging methods, the current efforts are focused on the synthesis of biocompatible and biodegradable platforms, as well as enhancement of the quantum efficiency, signal-to-background ratio, and fluorescence lifetime. *Ansari et al.* have addressed the pre-clinical applications of UCNP-based nanomedicine for diagnostic imaging in a recent review.[30]

Sun et al. reported the synthesis of mesoporous silica ($mSiO_2$)-coated $NaYF_4$:Yb,Tm@$NaGdF_4$ nanoparticles additionally grafted with lanthanide β-diketonate derivatives applying alkoxysilane-modified dibenzoylmethane (dbm-Si).[106] Moreover, they synthesized various UCNPs@$mSiO_2$-Ln(dbm)$_4$ (Ln^{3+} = Eu, Sm, Er, Yb, and Nd). The Eu^{3+}-containing hybrid material was subsequently successfully employed for multiple imaging modes including *in vitro* cell imaging upon 405 nm excitation, then for both *in vivo* and *ex vivo* small animal imaging upon 980 nm excitation. Furthermore, their potential as contrast agents in magnetic resonance imaging (MRI) was introduced due to the enhanced MR signal owing to the

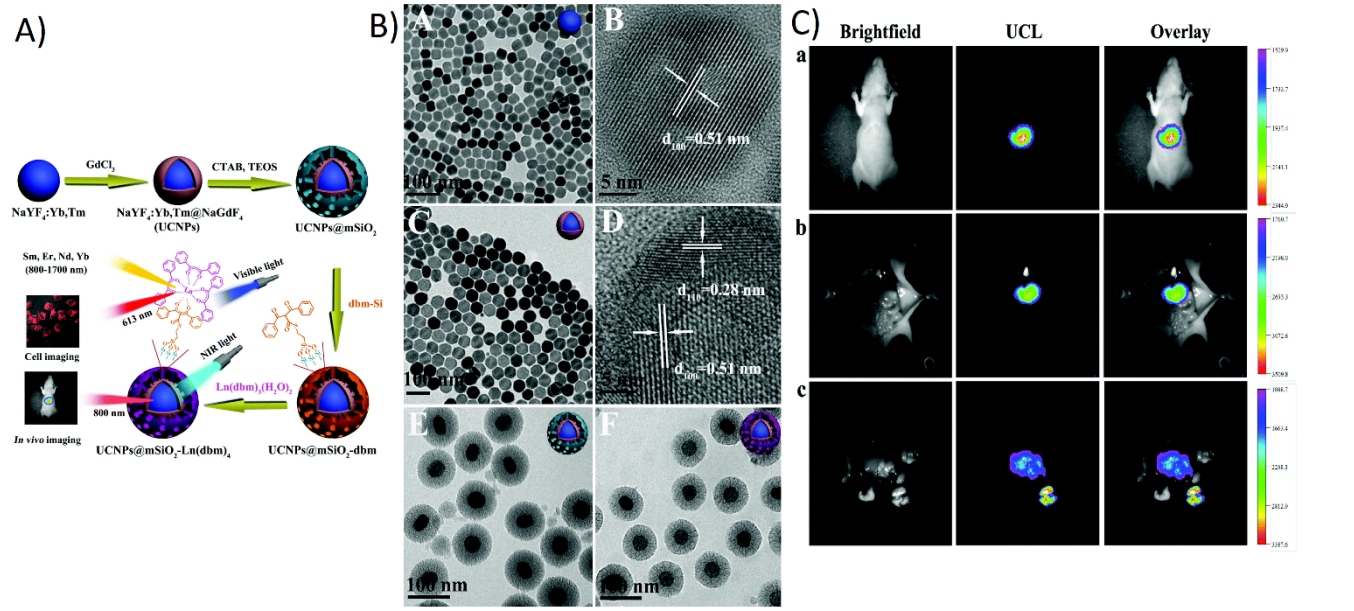

Figure 9 A) Synthetic route of UCNPs@mSiO$_2$-Ln(dbm)$_4$ (Ln = Eu, Sm, Er, Nd, Yb) and their consecutive imaging applications; B) TEM and HRTEM images of: NaYF$_4$:Yb,Tm (A and B), TEM and HRTEM images of: NaYF$_4$:Yb,Tm@NaGdF$_4$ (UCNPs) (C and D); TEM image of UCNPs@mSiO$_2$ (E), and TEM image of UCNPs@mSiO$_2$-Eu(dbm)$_4$ (F); and **C)** a) *in vivo* (top row), b) *in situ* (middle row), and c) *ex vivo* (bottom row) UCL imaging of a mouse. Reproduced from Reference [106], with permission from Royal Society of Chemistry.

magnetic properties of the Gd^{3+}-ions incorporated in the nanoparticle shell (Fig.9).

Temperature sensing

Ratiometric upconversion nanothermometers of core-shell type have been applied for *in vitro* and *in vivo* temperature sensing studies due to the relationship between the luminescence intensity ratio of two metastable intermediate states in Boltzmann equilibrium and the temperature-dependent population of those states.[23]

When it comes to hybrid silica-based nanothermometry systems, *Xu et al.* have reported the synthesis of NaYF$_4$:Yb,Er@NaYF$_4$@mSiO$_2$ nanocomposite loaded with ruthenium complex $[Ru(dpp)_3]^{2+}Cl_2$ in the mesoporous silica shell.[107] This nanocomposite was exploited in dual-operation mode, its green upconversion luminescence for temperature sensing upon excitation at 980 nm (λ_{em1} = 525 nm, λ_{em2} = 544 nm), and red downconversion luminescence (λ_{ex} = 455 nm, λ_{em} = 606 nm) for sensing of molecular O_2. The sensitivity range of the nanocomposite was found to be from 0.00325–0.00363 %/K in the physiological temperature range of 298-318 K. Furthermore, the nanocomposite was found to be with low cytotoxicity to *in vitro* cultured HepG-2 cells and was used for dual-mode cell imaging. *Zheng et al.* have synthesized NaGd(WO$_4$)$_2$:Yb^{3+}-Er^{3+}@SiO$_2$ core-shell nanoparticles and investigated the temperature sensing properties of the system in the physiological range of 300-350 K under 980 nm excitation. They showed that upon coating of the upconversion nanoparticles with a silica shell, the absolute sensitivity of the system increased almost two-fold with maximum S_a = 1.03 %/K at 350 K, and maximum S_r = 1.10 %/K at 300 K ($^2H_{11/2}/^4S_{3/2}$), as compared to maximum S_a = 0.66 %/K at 350 K, and maximum S_r = 0.98 %/K at 300 K for the bare NaGd(WO$_4$)$_2$:Yb^{3+}-Er^{3+} ($^2H_{11/2}/^4S_{3/2}$), respectively.[108]

Synthesis of multifunctional upconversion $Gd_2(WO_4)_3$:Yb^{3+}-Ho^{3+}@SiO$_2$ nanoparticles has been reported by *Liu et al.*[109] They further functionalized the particles with cis,cis,trans-diamminedichlorodisuccinatoplatinum(IV) drug or (DSP), and polyethylene glycol (PEG). Afterwards, the group investigated the temperature sensing properties of the $Gd_2(WO_4)_3$:Yb^{3+}-Ho^{3+}@SiO$_2$-Pt-PEG under 980 nm excitation in the physiological range and subsequently exploited them for bi-modal upconversion fluorescence (UCL) and magnetic resonance (MR) imaging, as well as for *in vitro* and *in vivo* investigation of the chemotherapeutic activity of the platinum(IV) drug in comparison with cisplatin. It was found that they exhibit a good

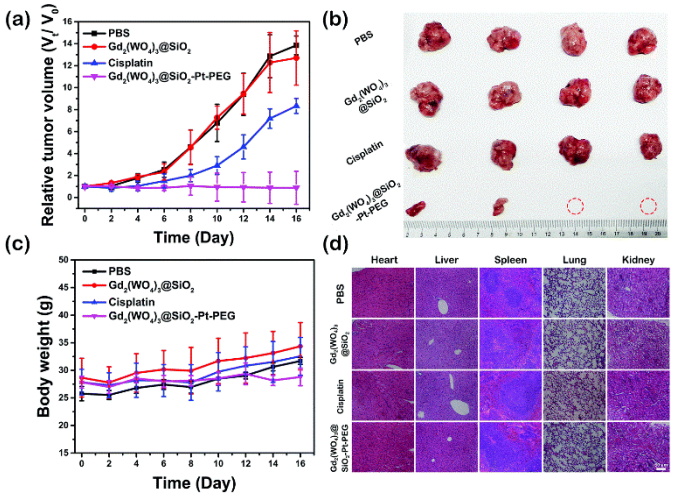

Figure 10 *In vivo* chemotherapy of $Gd_2(WO_4)_3$@SiO$_2$-Pt-PEG. (a) The changes of tumor sizes with time and with different treatments; (b) digital photographs of excised tumors with different treatments; (c) the changes of mice body weights with time and with different treatments; (d) the hematoxylin and eosin (H&E)-stained images of major organs after different treatments: PBS, cisplatin, $Gd_2(WO_4)_3$@SiO$_2$ and $Gd_2(WO_4)_3$@SiO$_2$-Pt-PEG. For more details, we refer the reader to the original publication. Reproduced from Reference [109], with permission from Royal Society of Chemistry.

contrast agent effect because of the Gd-presence and effective inhibition of CT26 cancer cells viability and tumor growth in mice, both *in vitro* and *in vivo* respectively (Fig.10). These investigations highlight the potential that hybrid silica-based nanomaterials hold for efficient applications in multimodal platforms.

Photodynamic and photothermal therapy and drug delivery

These two essentially different therapeutic approaches are mainly discussed in terms of cancer treatment and are usually introduced as novel alternatives to traditional chemotherapy, radiotherapy, and surgical procedures.[5] Moreover, they are often considered in terms of drug encapsulation, drug transport, and release as modalities which are exploited to trigger the release of an encapsulated drug by material disintegration or initiate hyperthermia on-demand for therapeutic purposes, respectively. This can be performed by effective localization of the nanoentities within the affected area either by direct intra-tumoral injection or by intra-venous injection.

In systems possessing photodynamic modality, external stimuli (e.g., light irradiation, magnetic field, etc.) are applied to initiate the process which subsequently influences the cancer cells microenvironment. The general physicochemical process of PDT involves three main steps: irradiation of the system, excitation of the photosensitizer (PS) component, and formation of cytotoxic reactive oxygen species (ROS) such as singlet oxygen ($^1O_2$), radical anions, and hydrogen peroxides.[110] These species then as highly reactive moieties damage the tumor cells membranes and constituents resulting in therapeutic, anticancer effect by means of apoptosis, necrosis, and/or autophagy.[111] The irradiation light intensity and wavelength should be chosen as to not irreversibly destroy the healthy tissue and be able to penetrate deep within the biomedium even to remote locations. For reasons discussed previously, NIR irradiation is usually applied, however, one major issue is the hypoxic tumor microenvironment which can significantly limit the formation of singlet oxygen ($^1O_2$) from molecular tumor oxygen (O_2). To combat this drawback, new PDT platforms with self-incorporated oxygen are being developed. This has also been applied with hybrid lanthanide-doped hollow mesoporous silica upconversion nanoparticles as a photocatalyst with the ability to generate in situ O_2 from H_2O_2, additionally encapsulating a load of a chemotherapeutic medicine doxorubicin (DOX) for simultaneous therapy (Fig.11).[112]

Idris et al. have reported a synthesis of $NaYF_4$:Yb-Er UCNPs coated with mesoporous silica additionally co-loaded with two photosensitizing components, merocyanine 540 (MC540) and zinc(II) phtalocyanine (ZnPc) for enhanced photothermal therapy.[113] Upon irradiation at 980 nm, both photosensitizers were activated through the green and red emissions of the core respectively for both *in vitro* cell viability tests and efficient *in vivo* PDT of melanoma-bearing mice. The dual-sensitizer

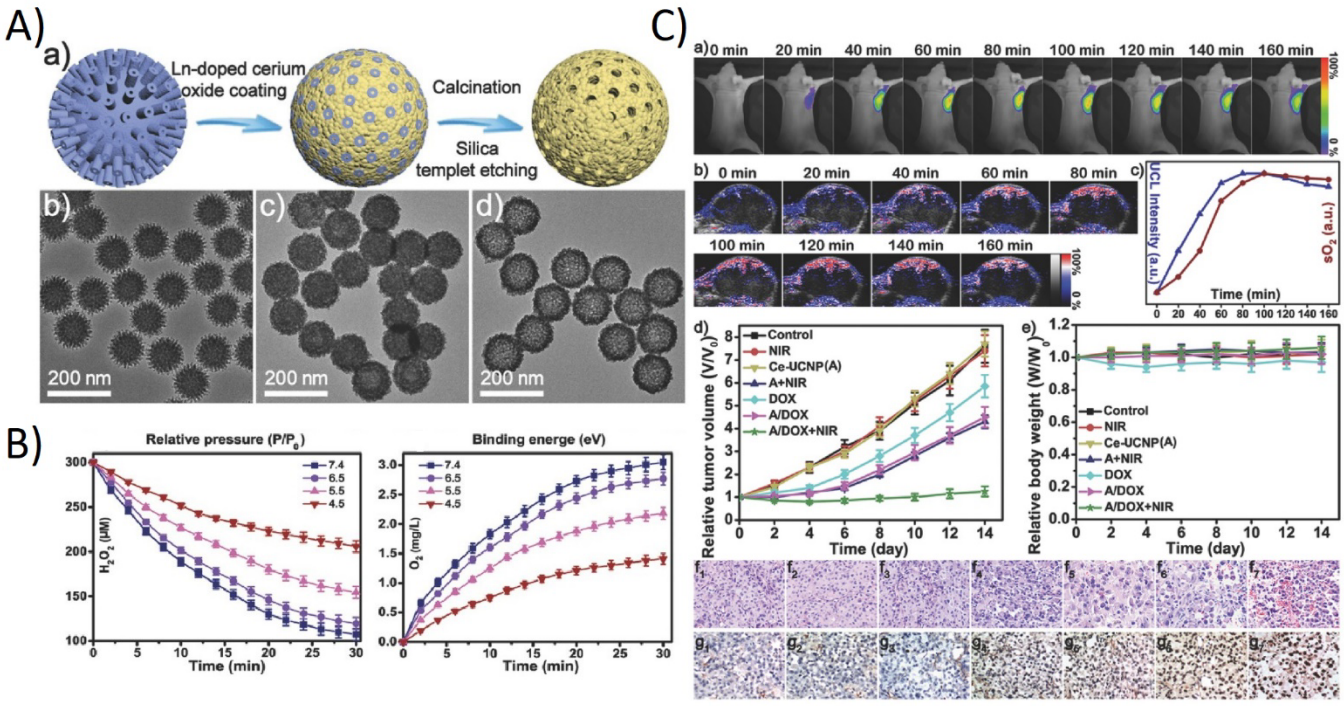

Figure 11 A) Illustration of the synthetic process of Yb^{3+}/Tm^{3+} co-doped mesoporous hollow Ce-UCNPs. TEM images of: b) initial silica template; c) silica with Yb^{3+}/Tm^{3+} co-doped Ce-UCNPs and d) mesoporous hollow Ce-UCNPs after calcination and silica etching processes. B) Plots: left - decomposition of H_2O_2 and right - generation of O_2 by Ce-UCNPs catalysis upon 30 min in aqueous solution. C) a) UC bioimaging of tumor in mice, b) representative images of solid tumors, c) quantification of bioimaging and and blood oxygen saturation in a) and b), d) tumor growth curves after various treatments. 1) Saline; (2) 20 min 980 nm NIR irradiation; (3) 100 min postinjection of Ce-UCNPs; (4) 100 min postinjection of Ce-UCNPs and 20 min 980 nm NIR irradiation; (5) 100 min postinjection of DOX (0.1 mg mL^{-1}, 200 µL per animal); (6) 100 min postinjection; (7) 100 min postinjection of DOX loaded Ce-UCNPs and 20 min 980 nm NIR irradiation. e) Relative body weight of mice after the above various treatments within 14 d. f_1–f_7) H&E and g_1–g_7) TUNEL staining of U87MG solid tumors after the above various treatments. We refer the reader to the original publication for details. Adapted from Reference [112], with permission from John Wiley and Sons.

approach exhibited a higher antitumor effect by the enhanced generation of singlet oxygen ($^1O_2$) as compared to a mono-sensitizer method.

Wang et al. synthesized hybrid nanoparticles of core-shell-shell type, namely $NaYF_4$:Yb,Er@SiO_2(MB)@mSiO_2-β-cyclodextrin where the mesoporous shell was loaded with rhodamine blue (RhB) as a model drug for drug delivery, and the inner solid silica shell contained photosensitizer methylene blue (MB) to trigger the photothermal therapy.[114] Cyclodextrin was applied as the gatekeeper of the pores. Under 980 nm excitation, it was shown that the red emission of the core at 660 nm activates the photosensitizer molecules, which consequently initiate the $^1O_2$ generation responsible for the anticancer PDT effect. This additionally disintegrates the cyclodextrin from the surface opening the pores for the intended drug release. Moreover, the green emission of the core at 540 nm was exploited for cell imaging thus achieving a triple-mode, cascade-like exploitable nanoplatform.

A relatively efficient drug loading and release platform for DOX and curcumin (CCM) as model drugs was reported by *Reddy et al*.[115] DOX- and CCM-loaded upconversion $NaYF_4$:Yb,Er@mSiO_2 nanoparticles both showed a pH-dependent drug release and inhibited the viability of *in vitro* cultured HeLa cells in a dose-dependent manner.

Another nanocomposite utilized for drug delivery is the LaF_3:Yb,Er@mSiO_2 prepared by *Yang et al*.[116] Ibuprofen was incorporated into the pores of the mSiO_2 shell as a model drug, its release was initiated by 980 nm excitation and was followed by UV-Vis spectroscopy.

Photothermal therapy (PTT), on the other hand, relies on an alternate mechanism. It involves the exploitation of photothermal transducing agents (PTAs) which capture the irradiation energy and transform it into localized heat consequently used for hyperthermic treatment of cancer cells. Metallic nanostructures are generally used for this purpose because of the garnered localized surface plasmon resonance (LSPR) effect where the oscillations of electrons are converted and given off as heat to the environment. Among the organic and inorganic species used as PTAs, the gold nanorods (GNRs) have the most advantageous features as their maximum absorbance can be tuned to occur within the first biological window (BW-I: 650-950 nm) by adjustment of their dimensions which aligns their surface plasmon resonance peak in BW-I.[110] GNRs can be utilized incorporated with upconversion nanoparticles into platforms that will simultaneously offer temperature sensing and drug-carrying moiety.

There are many reports on upconversion nanoparticles coupled with various gold species showing the promising theranostic potential of such hybrid materials. A study by *Zhang et al*. reporting $NaYF_4$:Yb^{3+}-Er^{3+}@$NaYF_4$ conjugate with GNRs has shown efficient simultaneous temperature sensing and photothermal conversion under 808 nm irradiation.[117] Another study involving upconversion $NaYF_4$:Yb^{3+}-Er^{3+}@$NaYF_4$@silica (core-shell-shell) nanoparticles decorated with gold nanoparticles has reported the enhanced cytotoxicity of such nanocomposite under NIR-radiation towards neuroblastoma cells via photothermal damage.[118] *Cai et al*. have reported synthesis of $NaGdF_4$:Yb/Er@$NaGdF_4$@SiO_2 upconversion multifunctional nanocomposite further coated with AuNPs into a $NaGdF_4$:Yb/Er@$NaGdF_4$@SiO_2@Au 3D species for drug delivery. The nanocomposite was also loaded with DOX as a model drug and was found to be biocompatible with enhanced drug release efficiency under 980 nm irradiation.[119] Such studies further strengthen the application of hybrid materials for multimodal functions for both *in vitro* and *in vivo* applications. Synergistic study of both PDT and PTT has also been reported by *Cen et al*.[120] They synthesized upconversion $NaYF_4$:Yb,Er,Tm@SiO_2-MB@PDA nanoprobes where the silica shell was loaded with photosensitizer methylene blue (MB) and the PDA acted as moiety with a binding affinity toward single-stranded DNA resulting in a hairpin probe with ability to bind cancer mRNAs. Under excitation at 980 nm, the emission at 655 nm was used to initiate the PDT, while the 800 nm emission was used for PTT simultaneously. This was verified by *in vitro* cell viability assays.

A major issue is the stability and robustness of materials exploited for drug delivery. The goal is to prepare a sufficiently stable, robust, and biocompatible platform that will endure the entire drug delivery process, as well as successfully modulate all the incorporated modalities and ideally disintegrate in a safe and non-invasive manner or will be removed from the organism through the usual removal routes. For example, the very robust PMO-based nanocarriers manifest enhanced biocompatibility due to the introduced organic groups within the intertwined inorganic-organic framework and their pH-dependent biodegradability has been reported in various studies.[121] This is a major triumph of impending hybrid materials over most of the classical purely inorganic UCNPs which do not possess such features.

Many issues yet remain and need to be resolved for both PDT and PTT, starting from efficient light penetration into deep tissue to reach inaccessible tumors, on to efficient and high drug loading and releasing capacity, to efficient excitation of the PSs and the PTAs respectively, to *in vivo* specific targeting of cells and tissues.

Nowadays, various catheter-type endoscopic devices are being developed such as optic fibers and nanofibers that can be implanted near the tumor sites and possess an ability to map the affected tissue, perform a biopsy, and carry theranostic agents to remote locations.[110] These devices represent a promising firsthand translation of nanotheranostics into clinical practice still exposed to the possibility of major improvements.

9. Conclusions and perspectives

There is no doubt that the future holds great potential for multifunctional hybrid silica-based lanthanide-doped UC luminescent nanothermometers in theranostics that will exhibit multimodal behavior for clinical and biomedical purposes, and towards personalized medicine. Such all-in-one simultaneous performance will be achieved by the combination of their *in vivo* and *ex vivo* optical (bio)imaging properties for diagnosis with their inherent temperature sensing modality characterized by high optical, spatial, and thermal resolution and sensitivity for

tracing, precise localization, and mapping of affected tissues differentiated by subtle temperature gradients. Moreover, the nanothermometers show advantageous characteristics over the traditionally used temperature measurement devices with improved sensitivity, resolution, and non-invasiveness. Additionally, their imminent application potential as nanoagents able to host and be coupled with photothermal transducing agents (PTAs) in photothermal therapies (PTT), and photosensitizing components (PSs) in photodynamic therapies (PDT), and even multi-mode therapies, proves attractive for impending cancer research and theranostics. Many studies done in the last decade show optimism for pending research into this complex topic. However, the successful clinical translation of such state-of-the-art theranostic liaisons is far from trivial because there are still significant challenges to be overcome before these nanovehicles earn the confidence of medical professionals and particularly of affected patients. Eliminating existing drawbacks and optimizing performance parameters is not a task of a specific field and profession, but a collaborative and progressively unifying mission of scientists, engineers, and medical professionals in multiple scientific, technological, and industrial fields. Synchronizing efforts in battling major diseases through safe, reliable, and innovative platforms gives promise that the ultimate benefit and achievement will be not that of a single individual and discipline, but of the universal healthcare and the entire humankind.

Author Contributions

S.P. (Chapters 1-3, 7-9) and M.L. (Chapters 4-6) did the literature search, wrote the draft of the manuscript, and prepared all figures included in it. A.M.K. provided guidance and feedback in the writing, as well as reviewing and editing of the manuscript. A.M.K. also provided funding to carry out this work.

Conflicts of interest

The authors declare no conflict of interest.

Acknowledgments

This work is part of a project that has received funding from the European Research Council (ERC) under the European Union's Horizon 2020 research and innovation programme (Grant agreement No. 945945).

References

1 Y. Houdas and R. E. F. J., *Human body temperature: Its measurement and Regulation*, Plenum, New York, 1982.
2 B. B. Lahiri, S. Bagavathiappan, T. Jayakumar and J. Philip, *Infrared Phys. Technol*., 2012, **55**, 221–235.
3 G. M. Cooper, *The cell a molecular approach*, Sinauer Associates, an imprint of Oxford University Press, New York, 2019.
4 L. Villarreal, O. Méndez, C. Salvans, J. Gregori, J. Baselga and J. Villanueva, *Mol. Cell Proteomics*, 2013, **12**, 1046–1060.
5 X. Y. Wong, A. Sena-Torralba, R. Álvarez-Diduk, K. Muthoosamy and A. Merkoçi, *ACS Nano*, 2020, **14**, 2585–2627.
6 C. Stefanadis, C. Chrysohoou, D. B. Panagiotakos, E. Passalidou, V. Katsi, V. Polychronopoulos and P. K. Toutouzas, *BMC Cancer*, 2003, **3**.
7 A. L. Shada, L. T. Dengel, G. R. Petroni, M. E. Smolkin, S. Acton and C. L. Slingluff, *J. Surg. Res.,* 2013, **182**.
8 A. Shimatani, M. Hoshi, N. Oebisu, N. Takada, Y. Ban and H. Nakamura, *Int. J. Clin. Oncol.,* 2021, 1-10.
9 L. Kennedy, J. K. Sandhu, M.-E. Harper and M. Cuperlovic-Culf, *Biomolecules*, 2020, **10**, 1429.
10 J. van der Zee, Ann. Oncol., 2002, 13, 1173–1184.
11 E. A. Repasky, S. S. Evans and M. W. Dewhirst*, Cancer Immunol. Res.,* 2013, **1**, 210–216.
12 G. Dranoff, *Nat. Rev. Cancer*, 2004, **4**, 11–22.
13 X.-F. Yang, J. H. Chang and S. M. Rothman, *Epilepsy Res*., 2002, **52**, 97–105.
14 R. Lasanen, E. Piippo-Savolainen, T. Remes-Pakarinen, L. Kröger, A. Heikkilä, P. Julkunen, J. Karhu and J. Töyräs, *Physiol. Meas.,* 2015, **36**, 273–282.
15 P. H. Lin, A. Echeverria and M. J. Poi, *J. Vasc. Surg. Cases Innov. Tech.,* 2017, **3**, 112–114.
16 J. Philip, T. Jayakumar, B. Raj, R. Karunanithi, T. M. R. Panicker, M. P. Korath, K. Jagadeesan, S. Bagavathiappan and T. Saravanan, *J. Med. Phys*., 2009, **34**, 43.
17 M. Dramićanin, *Luminescence thermometry: Methods, materials, and applications*, Woodhead Publishing, an imprint of Elsevier, Duxford, United Kingdom, 2018.
18 C. P. R. N., *Practical temperature measurement*, Butterworth-Heinemann, Oxford, Great Britain, 2001.
19 H. Amiri and B. Makkiabadi, *Front. Biomed. Technol.*, 2020, **7**, 82-91.
20 H. Odéen and D. L. Parker, Prog. Nucl. Magn. Reason. Spectrosc., 2019, **110**, 34–61.
21 A. Hakim and R. N. Awale, *J. Med. Syst.,* 2020, **44**.
22 C. D. Brites, S. Balabhadra and L. D. Carlos, *Adv. Opt. Mater.,* 2018, ***7***, 1801239.
23 D. Jaque and F. Vetrone, *Nanoscale*, 2012, **4**, 4301.
24 A. Bednarkiewicz, L. Marciniak, L. D. Carlos and D. Jaque, *Nanoscale*, 2020, **12**, 14405–14421.
25 G. Chen, H. Qiu, P.N. Prasad, X. Chen, *Chem. Rev.,* 2014, 114, **10**, 5161–5214.
26 F. Auzel, *Chem. Rev.,* 2004, 104, 1, 139–174.
27 E. Favilla, G. Cittadino, S. Veronesi, M. Tonelli, S. Fischer, J. C. Goldschmidt, A. Cassanho and H. P. Jenssen, *Sol. Energy Mater. Sol. Cells*, 2016, **157**, 415–421.
28 Z. Wang and A. Meijerink, *J. Phys. Chem. C*, 2018, **122**, 26298–26306.
29 A. A. Ansari, A. K. Parchur, M. K. Nazeeruddin and M. M. Tavakoli, *Coord. Chem. Rev.,* 2021, **444**, 214040.
30 A. A. Ansari, A. K. Parchur, N. D. Thorat and G. Chen, *Coord. Chem. Rev.,* 2021, **440**, 213971.
31 H. Dong, S.-R. Du, X.-Y. Zheng, G.-M. Lyu, L.-D. Sun, L.-D. Li, P.-Z. Zhang, C. Zhang and C.-H. Yan, *Chem. Rev.*, 2015, **115**, 10725–10815.
32 M. Lin, Y. Zhao, S. Q. Wang, M. Liu, Z. F. Duan, Y. M. Chen, F. Li, F. Xu and T. J. Lu, *Biotechnol. Adv.,* 2012, **30**, 1551–1561.
33 A. Ćirić, S. Stojadinović and M. D. Dramićanin, *Opt. Mater.,* 2018, **85**, 261–266.
34 M. Jia, G. Liu, Z. Sun, Z. Fu and W. Xu, *Inorg. Chem.,* 2018, **57**, 1213–1219.
35 W. Piotrowski, K. Kniec and L. Marciniak, *J. Alloys Compd.,* 2021, **870**, 159386.
36 Q. Dou and Y. Zhang, *Langmuir*, 2011, **27**, 13236–13241.
37 M. Suta and A. Meijerink, *Adv. Theory Simul.,* 2020, **3**, 2000176.

38 C. Bouzigues, T. Gacoin and A. Alexandrou, *ACS Nano*, 2011, **5**, 8488–8505.
39 A. Skripka, D. Mendez-Gonzalez, R. Marin, E. Ximendes, B. del Rosal, D. Jaque and P. Rodríguez-Sevilla, *Nanoscale Adv.,* 2021, **3**, 6310–6329.
40 A. Ortega-Rodríguez, Y. Shen, I. Zabala Gutierrez, H.D. Santos, V. Torres Vera, E. Ximendes, E., J. Rubio-Retama, *ACS Appl. Mater. Interfaces*, **12***,* 2020, *12* 12500-12509.
41 D. Ruiz, B. del Rosal, M. Acebrón, C. Palencia, C. Sun, J. Cabanillas-González, B.H. Juarez, B. H., *Adv. Funct. Mater.*, 2017, 27, **6**, 1604629.
42 G. M. Dalpian and J. R. Chelikowsky, *Phys. Rev. Lett.* 2006, **96**.
43 J. Liu, H. Rijckaert, M. Zeng, K. Haustraete, B. Laforce, L. Vincze, I. Van Driessche, A. M. Kaczmarek and R. Van Deun, *Adv. Funct. Mater.,* 2018, **28**, 1707365.
44 H. Suo, X. Zhao, Z. Zhang and C. Guo, *Chem. Eng. J.,* 2020, **389**, 124506.
45 G. S. Ofelt, *J. Chem. Phys*., 1962, **37**, 511–520.
46 B. R. Judd, *Phys. Rev.,* 1962, **127**, 750–761.
47 F. Wang, J. Wang and X. Liu, *Angew. Chem. Int. Ed.,* 2010, **49**, 7456–7460.
48 F. Wang, Y. Han, C. S. Lim, Y. Lu, J. Wang, J. Xu, H. Chen, C. Zhang, M. Hong and X. Liu, *Nature*, 2010, **463**, 1061–1065.
49 R. Shi, C. D. Brites and L. D. Carlos, *Nanoscale*, 2021.
50 D. T. Klier and M. U. Kumke, *J. Mater. Chem. C,* 2015, **3**, 11228–11238.
51 K. A. Abel, J.-C. Boyer and F. C. van Veggel, *J. Am. Chem. Soc.,* 2010, **132**, 5533–5533.
52 A. Kar and A. Patra, *Nanoscale*, 2012, **4**, 3608.
53 F. de Ferreira, A. J. de Morais, C. M. Santos Calado, F. Iikawa, O. D. Couto Junior, G. Brunet, M. Murugesu, I. O. Mazali and F. A. Sigoli, *Nanoscale*, 2021, **13**, 14723–14733.
54 Q. Dou, N. M. Idris and Y. Zhang, *Biomaterials*, 2013, **34**, 1722–1731.
55 F. Vetrone, R. Naccache, V. Mahalingam, C. G. Morgan and J. A. Capobianco, *Adv. Funct. Mater.,* 2009, **19**.
56 A. M. Kaczmarek, M. Suta, H. Rijckaert, T. P. van Swieten, I. Van Driessche, M. K. Kaczmarek and A. Meijerink, *J. Mater. Chem. C*, 2021, **9**, 3589–3600.
57 Z. Li and Y. Zhang, *Angew. Chem.,* 2006, **118**, 7896–7899.
58 L. Zhao, J. Peng, Q. Huang, C. Li, M. Chen, Y. Sun, Q. Lin, L. Zhu and F. Li, *Adv. Funct. Mater.,* 2013, **24**, 363–371.
59 R. Lv, D. Wang, L. Xiao, G. Chen, J. Xia and P. N. Prasad, *Sci. Rep.,* 2017, **7**.
60 W.-S. Lo, W.-T. Wong and G.-L. Law, *RSC Adv.,* 2016, **6**, 74100–74109.
61 Y.-F. Wang, G.-Y. Liu, L.-D. Sun, J.-W. Xiao, J.-C. Zhou and C.-H. Yan, *ACS Nano*, 2013, **7**, 7200–7206.
62 J. Shen, G. Chen, A.-M. Vu, W. Fan, O. S. Bilsel, C.-C. Chang and G. Han, *Adv. Opt. Mater.,* 2013, **1**, 644–650.
63 Q. Chen, C. Wang, L. Cheng, W. He, Z. Cheng and Z. Liu, *Biomaterials*, 2014, **35**, 2915–2923.
64 Q. Zhan, J. Qian, H. Liang, G. Somesfalean, D. Wang, S. He, Z. Zhang and S. Andersson-Engels, *ACS Nano*, 2011, **5**, 3744–3757.
65 L. Zhou, R. Wang, C. Yao, X. Li, C. Wang, X. Zhang, C. Xu, A. Zeng, D. Zhao and F. Zhang, *Nat. Commun.,* 2015, **6**.
66 M. Safdar, A. Ghazy, M. Lastusaari and M. Karppinen, *J. Mater. Chem. C*, 2020, **8**, 6946–6965.
67 W. Zou, C. Visser, J. A. Maduro, M. S. Pshenichnikov and J. C. Hummelen, *Nat. Photonics*, 2012, **6**, 560–564.
68 H. Zhang, Z.-H. Chen, X. Liu and F. Zhang, *Nano Res.,* 2020, **13**, 1795–1809.
69 J. Xu, P. Yang, M. Sun, H. Bi, B. Liu, D. Yang, J. Lin, ACS *nano*, 2017, **11**(4), 4133-4144.
70 W. Wei, G. Chen, A. Baev, G. S. He, W. Shao, J. Damasco and P. N. Prasad, *J. Am. Chem. Soc.,* 2016, **138**, 15130–15133.
71 P. Van Der Voort, D. Esquivel, E. De Canck, F. Goethals, I. Van Driessche and F. J. Romero-Salguero, *Chem. Soc. Rev.*, 2013, **42**, 3913–3955.
72 M. Li, S. Gul, D. Tian, E. Zhou, Y. Wang, Y. Han, L. Yin and L. Huang, *Dalton Trans.,* 2018, **47**, 12868–12872.
73 P. Su, X. Wang, T. Wang, X. Feng, M. Zhang, L. Liang, Y. Tang *Talanta*, 2021, 225, 122063.
74 Y. Li, J. Tang, L. He, Y. Liu, Y. Liu, C. Chen, C., Z. Tang, *Adv. Mat.*, 2015, *27*, **27**, 4075-4080.
75 Y. Shao, B. Liu, Z. Di, G. Zhang, L.D. Sun, L. Li, C.H. Yan, C. H., *ACS*, 2020, *142*, **7**, 3939-3946.
76 H.S. Jena, H. Rijckaert, C. Krishnaraj, I. Van Driessche, P. Van Der Voort, A.M. Kaczmarek, *Chem. of Mat.*, *33*, **20**, 8007-8017.
77 H. Rijckaert, S. Premcheska, S. Mohanty, J. Verduijn, A. Skirtach and A. M. Kaczmarek, *Phys. B: Condens. Matter*, 2021, 413453.
78 R. K. Sharma, P. Yadav, M. Yadav, R. Gupta, P. Rana, A. Srivastava, R. Zbořil, R. S. Varma, M. Antonietti and M. B. Gawande, *Mater. Horiz.,* 2020, **7**, 411–454.
79 A.M. Kaczmarek, *J. Mat. Chem. C*, 2018, **6**(22), 5916-5925.
80 A.M. Kaczmarek, Y.Y. Liu, M.K. Kaczmarek, H. Liu, F. Artizzu, L.D. Carlos, P. Van Der Voort, 2020, *Angew. Chem.*, **132**(5), 1948-1956.
81 P. Wang, F. Zhou, K. Guan, Y. Wang, X. Fu, Y. Yang, W. Tan, 2020, *Chem. Sci.*, **11**(5), 1299-1306.
82 A. M. Kaczmarek and P. Van Der Voort, *Materials*, 2020, **13**, 566.
83 B. Monteiro, J. P. Leal, R. F. Mendes, F. A. Almeida Paz, A. Linden, V. Smetana, A. V. Mudring, J. Avó and C. C. L. Pereira, *Mater. Chem. Phys.,* 2022, **277**, 125424.
84 A.M. Kaczmarek, R. Van Deun, P. Van Der Voort, *J. Material. Chem. C*, 2019, **7**(14), 4222-4229.
85 A.M. Kaczmarek, Y. Maegawa, A. Abalymov, A.G. Skirtach, S. Inagaki, P. Van Der Voort, *ACS Appl. Mater. Interfaces*, 2020, *12*(11), 13540-13550.
86 A. M. Kaczmarek, M. Suta, H. Rijckaert, A. Abalymov, I. Van Driessche, A. G. Skirtach, A. Meijerink and P. Van Der Voort, *Adv. Funct. Mater.,* 2020, **30**, 2003101.
87 M. S. Muthu, L. Mei and S.-S. Feng, *Nanomedicine*, 2014, **9**, 1277–1280.
88 22. M. S. Muthu, A. K. Mehata and M. K. Viswanadh, *Nanomedicine*, 2017, **12***,* 577–580.
89 D. Ghosh Dastidar and G. Chakrabarti, *Applications of Targeted Nano Drugs and Delivery Systems*, 2019, 133–155.
90 E.-K. Lim, T. Kim, S. Paik, S. Haam, Y.-M. Huh and K. Lee, *Chem. Rev.*, 2014, **115**, 327–394.
91 A. Mohapatra, S. Uthaman and I.-K. Park, *Front. Mol. Biosci.*, 2021, **7**.
92 C.L. Tsai, J.C. Chen, W.J. Wang, *J. Med. Biol. Eng.*, **21** (2001), pp. 7-14.
93 J. R. Mourant, J. P. Freyer, A. H. Hielscher, A. A. Eick, D. Shen and T. M. Johnson, *Appl. Opt.*, 1998, **37**, 3586.
94 E. Hemmer, P. Acosta-Mora, J. Méndez-Ramos and S. Fischer, *J. Mater. Chem. B*, 2017, **5**, 4365–4392.
95 Y. Shen, J. Lifante, E. Ximendes, H. D. Santos, D. Ruiz, B. H. Juárez, I. Zabala Gutiérrez, V. Torres Vera, J. Rubio Retama, E. Martín Rodríguez, D. H. Ortgies, D. Jaque, A. Benayas and B. del Rosal, *Nanoscale*, 2019, **11**, 19251–19264.
96 A. M. Kaczmarek, R. Van Deun and M. K. Kaczmarek, *Sens. Actuators B Chem.*, 2018, **273**, 696–702.
97 H. Huang, W. Feng, Y. Chen and J. Shi, *Nano Today*, 2020, **35**, 100972.
98 S. Thangudu, F.-Y. Cheng and C.-H. Su, *Polymers*, 2020, **12**, 3055.
99 X. Li, V. Vemireddy, Q. Cai, H. Xiong, P. Kang, X. Li, M. Giannotta, H. N. Hayenga, E. Pan, S. R. Sirsi, C. Mateo, D. Kleinfeld, C. Greene, M. Campbell, E. Dejana, R. Bachoo and Z. Qin, *Nano Lett.*, 2021, **21**, 9805–9815.

100 A. Bednarkiewicz, J. Drabik, K. Trejgis, D. Jaque, E. Ximendes and L. Marciniak, *Appl. Phys. Rev.*, 2021, **8**, 011317.
101 A. Nexha, J. J. Carvajal, M. C. Pujol, F. Díaz and M. Aguiló, *Nanoscale*, 2021, **13**, 7913–7987.
102 J. Zhou, B. del Rosal, D. Jaque, S. Uchiyama and D. Jin, *Nat. Methods*, 2020, **17**, 967–980.
103 C. Bharti, N. Gulati, U. Nagaich and A. K. Pal, *Int. J. Pharm. Investig.*, 2015, **5**, 124.
104 S. Simovic, N. Ghouchi-Eskandar, A. Moom Sinn, D. Losic and C. A. Prestidge, *Curr. Drug Discov. Technol.*, 2011, **8**, 250–268.
105 Y. Wang, Q. Zhao, N. Han, L. Bai, J. Li, J. Liu, E. Che, L. Hu, Q. Zhang, T. Jiang and S. Wang, *Nanomed.: Nanotechnol., Biol. Med.*, 2015, **11**, 313–327.
106 L. Sun, X. Ge, J. Liu, Y. Qiu, Z. Wei, B. Tian and L. Shi, *Nanoscale*, 2014, **6**, 13242–13252.
107 S. Xu, Y. Yu, Y. Gao, Y. Zhang, X. Li, J. Zhang, Y. Wang and B. Chen, *Microchim. Acta*, 2018, **185**.
108 L. Zheng, X. Huang, J. Zhong, Z. Wang and X. Cheng, *RSC Adv.*, 2021, **11**, 3981–3989.
109 G. Liu, Y. Chen, M. Jia, Z. Sun, B. Ding, S. Shao, F. Jiang, Z. Fu, P. Ma and J. Lin, *Dalton Trans.*, 2019, **48**, 10537–10546.
110 N. D. Thorat, S. A. Tofail, B. von Rechenberg, H. Townley, G. Brennan, C. Silien, H. M. Yadav, T. Steffen and J. Bauer, *Appl. Phys. Rev.*, 2019, **6**, 041306.
111 R. Mohammadinejad, M. A. Moosavi, S. Tavakol, D. Ö. Vardar, A. Hosseini, M. Rahmati, L. Dini, S. Hussain, A. Mandegary and D. J. Klionsky, *Autophagy*, 2018, **15**, 4–33.
112 C. Yao, W. Wang, P. Wang, M. Zhao, X. Li and F. Zhang, *Adv. Mater.*, 2018, **30**, 1704833.
113 N. M. Idris, M. K. Gnanasammandhan, J. Zhang, P. C. Ho, R. Mahendran and Y. Zhang, *Nat. Med.*, 2012, **18**, 1580–1585.
114 H. Wang, R.-Lu Han, L.-Ming Yang, J.-Hui Shi, Z.-Jun Liu, Y. Hu, Y. Wang, S.-Juan Liu and Y. Gan, *ACS Appl. Mater. Interfaces*, 2016, **8**, 4416–4423.
115 K. L. Reddy, P. K. Sharma, A. Singh, A. Kumar, K. R. Shankar, Y. Singh, N. Garg and V. Krishnan, *Mater. Sci. Eng. C*, 2019, **96**, 86–95.
116 Y. Yang, Y. Qu, J. Zhao, Q. Zeng, Y. Ran, Q. Zhang, X. Kong and H. Zhang, *Eur. J. Inorg. Chem*., 2010, **2010**, 5195–5199.
117 Y. Zhang, S. Xu, X. Li, J. Zhang, J. Sun, H. Xia, R. Hua and B. Chen, Mater. Res. Bull., 2019, **114**, 148–155.
118 L. P. Qian, L. H. Zhou, H.-P. Too and G.-M. Chow, J. Nanopart. Res., 2010, **13**, 499–510.
119 H. Cai, T. Shen, A. M. Kirillov, Y. Zhang, C. Shan, X. Li, W. Liu and Y. Tang, Inorg. Chem., 2017, **56**, 5295–5304.
120 Y. Cen, W.-J. Deng, Y. Yang, R.-Q. Yu and X. Chu, Anal. Chem., 2017, **89**, 10321–10328.
121 J. Croissant, X. Cattoën, M. Wong Chi Man, J. Durand and N. Khashab, Nanoscale, 2015, **7**, 20318-20334.